CHAPTER 5

INDUSTRIAL APPLICATIONS OF DIAMOND ELECTRODES

Werner Haenni and Philippe Rychen

CSEM SWISS CENTER OF ELECTRONICS AND MICROTECHNOLOGY INC., CH2007 NEUCHÂTEL, SWITZERLAND

Matthyas Fryda

CONDIAS GMBH, D-25524 ITZEHOE, GERMANY

Christos Comninellis

EPFL FEDERAL INSTITUTE OF TECHNOLOGY, CH-1500 LAUSANNE, SWITZERLAND

1. Diamond Electrodes: Specification

1.1. INTRODUCTION

The development of high-quality and wear-resistant anode materials for a wide range of processes such as electrosynthesis of organic and inorganic compounds, galvanic applications and treatment of effluents containing organic pollutants, present a serious challenge to electrochemists.

Highly efficient anodes for technical electrolysis must possess the following basic properties:

- Long-term chemical and electrochemical stability
- Good electric conductivity
- High selectivity for the desired reaction
- High electrocatalytic activity (low overpotential)
- Resistance to electrode deactivation and fouling
- Sufficient mechanical stability
- Technical feasibility of fabrication
- Acceptable cost

The long-term stability is the most important property, which must be realized for any industrial application. Electrode wear may lead to contaminated product and to additional costs due to the need for periodic replacement.

ISBN: 0-12-752186-0
ISSN: 0080-8784

During the last years the so-called dimensionally stable anodes (DSA®)[1] have been developed, both for Cl_2 production (DSA-Cl_2) and oxygen evolution in acid medium (DSA-O_2). These electrodes have the general structure:

- Conductive substrate/active layer

The valve metals: titanium, zirconium, niobium, tantalum and their alloys have been proposed as conductive substrates. However, titanium has primarily been used. The active layer is made of a few micrometer thick porous oxide film. RuO_2–TiO_2 oxide mixtures have been used for Cl_2 production (DSA-Cl_2) and IrO_2–Ta_2O_5 mixture for oxygen evolution (DSA-O_2). Although DSA-Cl_2 and the DSA-O_2 anodes have been successfully used for chlorine production and oxygen evolution, respectively, it seems that they are specific to these reactions. Furthermore, the DSA-O_2 anodes have low stability at high anodic current densities in acid media.

In this work we investigate a new type of DSA® electrodes based on a boron-doped diamond (BDD) active layer. The general structure of this electrode is:

- Conductive substrate/BDD

This type of electrode is expected to open new possibilities in industrial electrosynthesis, galvanic applications and water treatment.

In this section the possible conductive substrates are presented followed by a more detailed explanation of active electrode layers and surface modification.

1.2. Substrates for Diamond Electrodes

The basic criteria for a suitable substrate for anodes, cathodes and bipolar electrodes are:

Anodes	It must have valve characteristics (anodic passivation by formation of a dense non-conducting oxide).
Cathodes	It must resist hydrogen embrittlement.
Bipolar	Both anodic and cathodic operation must be possible.

The candidate substrates for the BDD coating can be classified into two main categories:

- Metallic substrates: valve metals (titanium, zirconium, niobium, tantalum and some of their alloys)
- Ceramic conductive substrates

[1] DSA®, Nafion®, DiaChem® and DiaCell® are registered names.

The substrate for BDD electrodes must also satisfy the following criteria inherent to the preparation conditions of the BDD coating according to the findings of these workers (Haenni and Fryda, 2000a):

- Chemical and mechanical stability at the preparation conditions of the BDD coating (950 °C, in H_2 atmosphere)
- Formation of a conductive layer (carbide) at the substrate/BDD interface
- Formation of a diffusion barrier to avoid hydrogen embrittlement (especially in case of valve metal substrates)
- Adequate thermal expansion coefficient

1.2.1. Metallic Substrates

If using metallic substrates, the metal must have valve characteristics (formation by anodic oxidation of an insulating compact oxide film). These are titanium (Fischer, Gandini, Laufer, Blank and Comninellis, 1998; Fryda, Hermann, Schäfer, Klages, Perret, Haenni, Comninellis and Gandini, 1999b), zirconium, niobium (Fryda et al., 1999b) and tantalum (Swain, 1994; Fryda et al., 1999b). Molybdenum (Swain, 1994; Ramesham, 1999a) and tungsten (Swain, 1994; Martin, Argoitia, Angus, Anderson and Landau, 1995; Sakharova, Pleskov, Di Quarto, Piazza, Sunseri, Teremetskaya and Varnin, 1995) have also been proposed.

In order to establish a comparison of these metallic substrates and the related carbides (formed at the metal/BDD interface), the following criteria have been taken into consideration:

- Economy (cost of substrates)
- Electrical conductivity and thermal expansion coefficients for both the metallic substrate and the related carbides (formed at the metal/BDD interface)
- Chemical stability for both the metallic substrate and the related carbides (formed at the metal/BDD interface)
- Hydrogen embrittlement, phase transformation at the working temperature for both the metallic substrate and the related carbides (formed at the metal/BDD interface)
- Capacity to form a diffusion barrier to avoid hydrogen embrittlement

Each substrate and the related carbides (formed at the metal/BDD interface) are evaluated following these criteria with points from 1 to 4 (4 is given for the most appropriate substrate).

In Table I the specific cost ($\$ m^{-2}$) of a typical valve metal of 1 mm thickness is compared. It can clearly be seen that titanium (4 points) is the lowest priced

TABLE I

SPECIFIC COST OF VALVE METAL SUPPORTS FOR METAL/BDD ELECTRODES

Element	Density (kg dm^{-3})	\$ kg^{-1}	\$ m^{-2}	Points
Titanium	4.5	110	880	4
Zirconium	6.5	130	940	3
Niobium	8.4	250	2180	2
Tantalum	16.6	440	7350	1

material followed directly by zirconium (3 points), whereas tantalum (1 point) is the most expensive.

Furthermore, mesh and grid materials as well as rods, tubes and cylinders can be obtained in titanium. Zirconium and niobium can also be obtained in the form of rods but all other shapes have to be ordered at extra cost.

In Table II the thermal expansion coefficients and the electrical resistivity for both the metallic substrates and the related carbides (formed at the metal/BDD interface) are given. The BDD values are also given for comparison.

Tantalum and niobium show the smallest thermal expansion coefficients and a lower electrical resistivity.

The chemical stability of these valve metals and the related interfaces are presented in Table III. Tantalum (4 points) followed by niobium (3 points) show a higher stability. The carbides of niobium and tantalum formed at the diamond coating temperature are partially stable in neutral and acid oxidizing medium, all other carbides are rapidly corroded. Finally, all valve metals and the corresponding carbides show limited stability in alkaline oxidizing medium as well in fluoride media.

TABLE II

THERMAL EXPANSION COEFFICIENTS AND ELECTRICAL RESISTIVITY OF BDD, VALVE METALS AND THE RELATED CARBIDES (FORMED AT THE METAL/BDD INTERFACE)

Element and interface	Thermal expansion coefficient 10^{-6} K^{-1} (293–1200 K)	Electrical resistivity (mΩ cm)	Points
Diamond (BDD)	1.0	8–50	
Titanium	8.82	0.042	2
Zirconium	9.92	0.041	1
Niobium	8.37	0.014	3
Tantalum	6.3	0.014	4
TiC	8.8	0.1	
ZrC	6.5	0.06–0.1	
NbC	7.29	0.15	
TaC	6.64	0.05–0.1	

TABLE III

CHEMICAL STABILITY (+: STABLE, −: UNSTABLE, 0: PARTIALLY STABLE) OF THE VALVE METALS AND THE RELATED CARBIDES (FORMED AT THE METAL/BDD INTERFACE) IN DIFFERENT MEDIA

Element and interface	H_2O_2 33%	H_2O_2, H_2SO_4	H_2O_2, NH_4OH	H_2O_2, KOH	HF	Points
Titanium	+	+	−	−	−	2
Zirconium	+	+	−	−	−	1
Niobium	+	+	−	−	−	3
Tantalum	+	+	−	−	−	4
TiC	−	−	−	−	0	
ZrC	−	−	−	−	−	
NbC	0	0	−	−	0	
TaC	0	0	−	−	0	

In Table IV the thermal stability of the valve metals and the related carbides (formed at the metal/BDD interface) are presented. The problem of all these valve metals, but especially titanium, is their tendency to hydrogen embrittlement. To avoid the hydrogen embrittlement during diamond deposition in a hydrogen atmosphere at high temperature, an interlayer acting as hydrogen diffusion barrier must be deposited on the metallic support prior to diamond deposition. Carbide interlayers are sufficient diffusion barriers against hydrogen. Finally, titanium and zirconium produce metallic phase transformations (α to β) at 920 and 863 °C, respectively. The diamond deposition temperature ordinarily is between 750 and 950 °C and is very close or even overlaps with the transformation temperature.

Adding all points in Table V permits one to establish a figure of merit for these valve metals including their interface components.

TABLE IV

HYDROGEN EMBRITTLEMENT AND PHASE TRANSFORMATION STABILITY (+: STABLE, −: UNSTABLE, 0: PARTIALLY STABLE) OF THE VALVE METALS AND THE RELATED CARBIDES (FORMED AT THE METAL/BDD INTERFACE)

Element and interface	Hydrogen embrittlement	Diffusion barrier	Phase transformation	Points
Titanium	−		α–β 920 °C	1
Zirconium	+		α–β 863 °C	2
Niobium	0			4
Tantalum	0			3
TiC		−		
ZrC		0		
NbC		0		
TaC		0		

TABLE V
FIGURE OF MERIT OF VALVE METAL SUPPORTS

Criteria	Ti	Zr	Nb	Ta
Cost	4	3	2	1
Contact	2	1	3	4
Chemical stab	2	1	3	4
Hydrogen and thermal stability	1	2	4	3
Total	9	7	12	12

The most attractive metallic supports are niobium and tantalum followed by titanium and zirconium. Following the initially defined criteria, all these valve metals can be used as anode supporting material for BDD electrodes.

1.2.2. Ceramic Conductive Substrates

All electrically conducting materials and composites, which are not metals or alloys, can be classified as conductive ceramic substrates. Typical examples are carbon allotropes and silicon:
Carbon allotropes:

- Graphite and pyrographite (Swain, 1994; Ramesham, 1999b)
- Hard carbon and pyrocarbon
- Glassy carbon (Swain, 1994)
- Carbon fiber reinforced composites

Silicon (Swain, 1994; Jiali, Jianzhong, Guoxiong, Xinru and Nianyi, 1996; Vinokur, Miller, Vinokur, Miller, Avyigal and Kalish, 1996; Katsuki, Takahashi, Toyoda, Kurosu, Lida, Wakita, Nishiki and Shimamune, 1998; Yano, Tryk, Hashimoto and Fujishima, 1998; Fryda et al., 1999b; Haenni and Fryda, 2000a):

- Monocrystalline, boron-doped silicon with an electrical resistivity of 1–10 mΩ cm
- Polycrystalline, boron-doped silicon
- Silicon coatings deposited on a compatible substrate

Mosaic shape supports electrodes. Diamond-coated silicon plates are soldered on sheets like titanium or aluminum (Haenni, Perret and Rychen, 2001b).

Table VI contains the main properties of the materials described above. The BDD values are also given for comparison.

TABLE VI

MAIN PROPERTIES OF BDD AND SELECTED CERAMIC CONDUCTIVE SUBSTRATES (+: STABLE, −: UNSTABLE). CARBON-BASED MATERIALS ARE THE ONLY MATERIALS SUITABLE AS CATHODIC SUBSTRATES FOR DIAMOND ELECTRODES, WHEREAS SILICON REMAINS THE ONLY ANODIC SUBSTRATE FOR DIAMOND ELECTRODES. ONLY DIAMOND IS STABLE UNDER BIPOLAR ELECTRODE CONDITIONS

Material	Thermal expansion coefficient 10^{-6} K^{-1} (293–1200 K)	Electrical resistivity (mΩ cm)	Anodic stability	Cathodic stability	Bipolar stability
BDD	1.5	8–50	+	+	+
Graphite	2.6–7.9	0.007–0.04	−	+	−
Glassy carbon	3.2–3.5	0.1–0.2	−	+	−
C-fiber/C	0.8–6.9	0.02–0.05	−	+	−
p-Si (Boron)	3.7	1–10	+	−	−

1.3. ACTIVE ELECTRODE LAYER

1.3.1. Boron-doped Diamond

The boron-doped, polycrystalline diamond films developed by the workers (Swain, 1994; Martin et al., 1995; Sakharova et al., 1995; Jiali et al., 1996; Vinokur et al., 1996; Fischer et al., 1998; Katsuki et al., 1998; Yano et al., 1998; Fryda et al., 1999b; Fu, Yan, Loh, Sun and Hing, 1999; Haenni and Perret, 1999b; Ramesham, 1999a,b; Beck, Kaiser and Krohn, 2000; Fu, Yan and Loh, 2000; Haenni and Fryda, 2000a; Haenni et al., 2001b) as well as homoepitaxially grown boron-doped monocrystalline diamond films as demonstrated by the workers (Densienko, Aleksov and Kohn, 2001) are the most frequently used active layers in conductive substrate/diamond electrode types.

The electrical resistivity of BDD films depends on the doping level of boron in the diamond coating. Figure 1 shows the influence of boron concentration (in the diamond coating) on the resistivity of the BDD film.

Typical and useful boron concentrations in diamond electrodes are from some 500 ppm to about 8000 ppm. At lower doping levels (<500 ppm) the electrical resistivity is too high for electrochemical applications; for boron-doping levels exceeding 8000 ppm the electrode is anodically consumed. This may be because at high-boron concentrations the secondary nucleation of diamond as well as the formation of sp^2 carbon species, essentially at the grain boundaries, is favored. Formation of boron carbide at the grain boundaries cannot be excluded at such high boron doping levels.

A typical cyclovoltammogram of BDD electrodes doped with 3000 ppm boron is shown in Figure 2 in acid and basic solutions as demonstrated by the workers (Swain, 1994; Martin et al., 1995; Sakharova et al., 1995; Perret, Haenni,

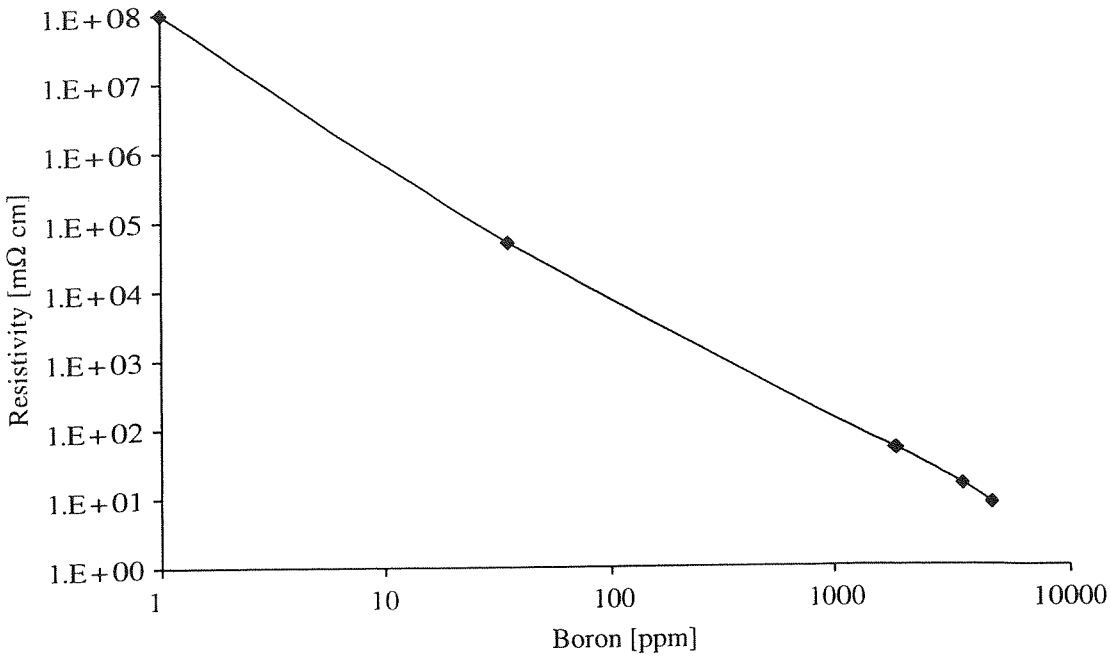

FIG. 1. Resistivity of BDD films as a function of the boron concentration in the diamond coating (CSEM data).

Niedermann, Skinner, Comninellis and Gandini, 1997; Fryda et al., 1999b; Abdelmula and Jüttner, 2001).

BDD electrodes, as grown in a hydrogen atmosphere, show hydrophobic surface behavior due to the hydrogen surface termination. If these electrodes are used as anodes at the potential of oxygen evolution, the BDD surface becomes hydrophilic.

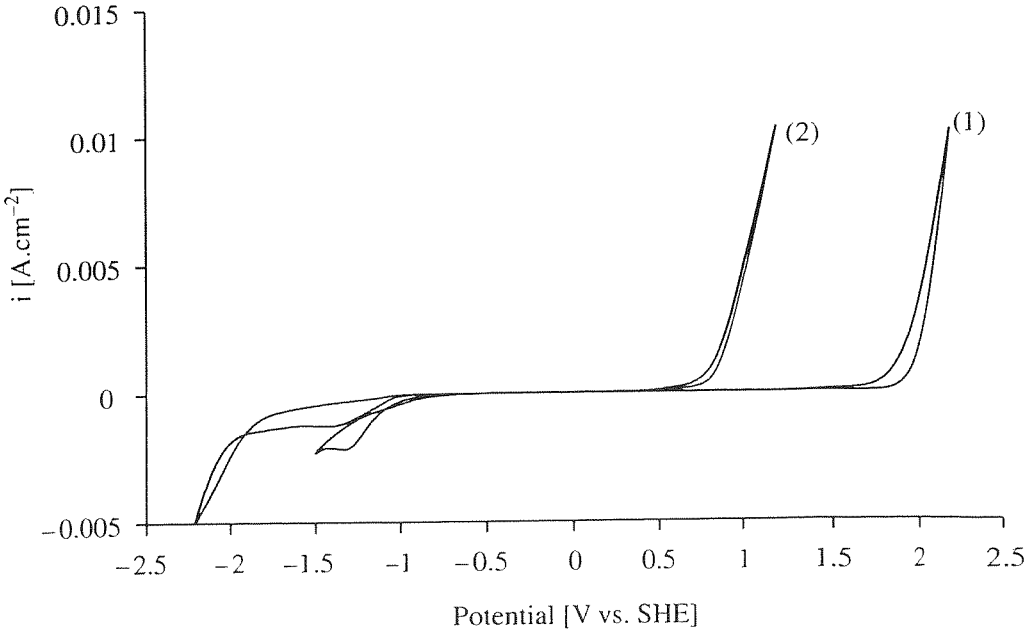

FIG. 2. Cyclovoltammogram of boron-doped diamond in (1) H_2SO_4 1 M, (2) KOH 1 M.

1.3.2. Nitrogen/Boron-co-doped Diamond (NBDD)

Diamond was deposited on p-Si substrates in the presence of both nitrogen (from ammonia) and boron dopants. The typical concentrations in the NBDD electrodes are 20–100 ppm for boron and 2–20 ppm for nitrogen. The electrical resistivity of these electrodes is 0.05–0.5 Ω cm. It is worth noting that the resistivity of a pure 20–100 ppm BDD (without nitrogen) is 10–100 Ω cm. These NBDD electrodes have an even larger electrochemical window than BDD (Fig. 3) as demonstrated by the workers (Haenni, Borel, Perret, Correa, Michaud and Comninellis, 1999a; Haenni and Fryda, 2000a; Haenni and Perret, 2000b).

As far as known to the authors, this is the first report of this type of NBDD electrodes. Further work is in progress for a better understanding of the conduction mechanism and the electrochemical behavior of this material. The authors (Yu, Miyamoto and Sugino, 2000) are proposing n-type doping of diamond by studying systems like N–Al–N, P–H–P and N–B–N.

Similar to the BDD electrodes, the NBDD electrodes show a hydrophobic surface, which is transformed to hydrophilic properties by anodic polarization.

1.3.3. Metal Oxide Modified Diamond Electrodes

Complex inner-sphere electrode reactions are generally very slow on BDD electrodes due to the poor adsorption capacity of the diamond surface.

Typical inner-sphere reactions are anodic oxygen evolution and cathodic hydrogen evolution. The slow kinetics of these reactions on BDD electrodes are the main reason for the wide potential window of BDD electrodes in aqueous media.

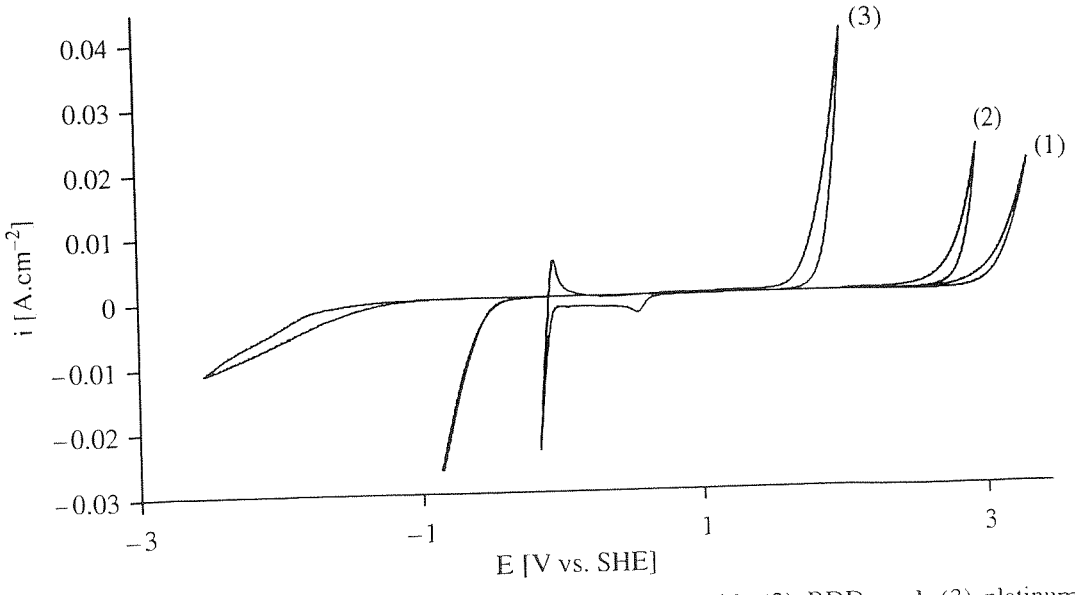

FIG. 3. Cyclovoltammogram of (1) NBDD in comparison with (2) BDD and (3) platinum in H_2SO_4 1 M.

In order to enhance the electrocatalytic activity of the BDD electrode, IrO_2 clusters have been deposited on the BDD surface (BDD–IrO_2 electrode) by these workers (Duo, Michaud, Haenni, Perret and Comninellis, 2000). It is well known that IrO_2 can act as redox catalyst in both oxygen evolution and organic oxidation reactions. IrO_2 has been deposited on the hydrophilic BDD surface by thermal decomposition. In a typical example, 5 μl of 2.2 mM $H_2IrCl_6 \cdot 6H_2O$ solution in isopropanol was applied to the BDD surface (1 cm^2), the solvent was evaporated at 80°C, then treated in a furnace during 1 h at 350°C in air. The calculated amount of IrO_2 deposited was 2.5 $\mu g\ cm^{-2}$.

Figure 4 shows cyclic voltammetric curves in 1 M H_2SO_4 at 20°C with a scan rate of 50 mV s^{-1} for (A) BDD and (B) BDD–IrO_2 electrodes.

The voltammetric curve for BDD–IrO_2 electrodes (2.5 μg IrO_2 cm^{-2}) shows that the current begins to increase at approximately 1.4 V (SHE) due to oxygen evolution. This potential coincides with the redox potential of the couple IrO_2/IrO_3.

This behavior of the BDD–IrO_2 electrodes is very similar to the continuous IrO_2 films obtained on Ti substrates (DSA-O_2). Thus, we can suggest a similar redox catalysis mechanism for oxygen evolution on BDD–IrO_2 electrodes.

According to this mechanism, adsorbed water on the IrO_2 clusters is discharged forming hydroxyl radicals in a first step, which interacts chemically with IrO_2 forming the higher oxide IrO_3.This step is followed by the chemical decomposition of the higher oxide IrO_3 to oxygen and IrO_2 according to the findings of these workers (Duo et al., 2000).

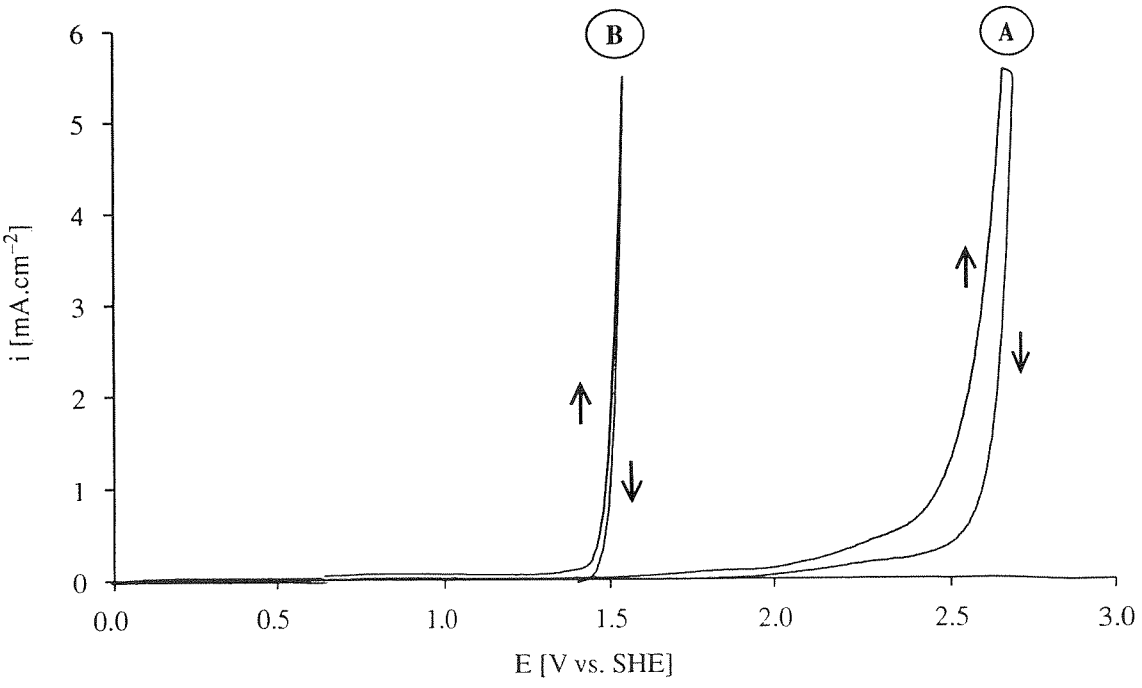

FIG. 4. Cyclic voltammetric curves in 1 M H_2SO_4 at 20 °C (A) BDD electrode, (B) BDD–IrO_2 electrode. Scan rate = 50 m s^{-1}. Reprinted with permission from: I. Duo, P.-A. Michaud, W. Haenni, A. Perret, and Ch. Comninellis, *Electrochem. Solid-State Lett.* 3 (7), 325 (2000). Copyright 2000. The Electrochemical Society Inc.

2. Fabrication Method

2.1. Large-scale Fabrication of BDD Electrodes

BDD electrodes are of interest for a wide range of electrochemical applications because of their unique properties. However, until now, diamond has not been introduced in industrial electrochemical applications because of the limited availability of diamond for large-area electrodes. During recent years, large-area hot-filament chemical vapor deposition (HF-CVD) of polycrystalline diamond films has been developed, yielding deposition areas of 0.5 m^2 on metallic and ceramic substrates.

The most important improvements of this HF-CVD process are:

- substrate pretreatment, e.g., by ultrasonic irradiation in a diamond powder suspension, increases the nucleation density considerably, leading to faster formation of a continuous film and better utilization of growth species in the early growth phase
- diamond can be deposited with increasing growth rates with methane concentrations from 0.1 to 3 vol% in hydrogen, with filament temperatures between 2300 and 2600 °C, with lower filament–substrate distances
- multifilament arrays allow large-area deposition.

Such multifilament arrays are not only suitable for the production of large-area electrodes but can also be used for the simultaneous coating of both electrode sides as well as complex-shaped electrodes by adaptation of the filament arrays for three-dimensional substrates (Fig. 5).

In a cooperation between Fraunhofer-IST, Germany, and CSEM, Switzerland, DiaChem® electrodes with reproducible electrochemical properties were produced on metallic (for example Ta, Ti, Mo, W, Zr), silicon, ceramic and

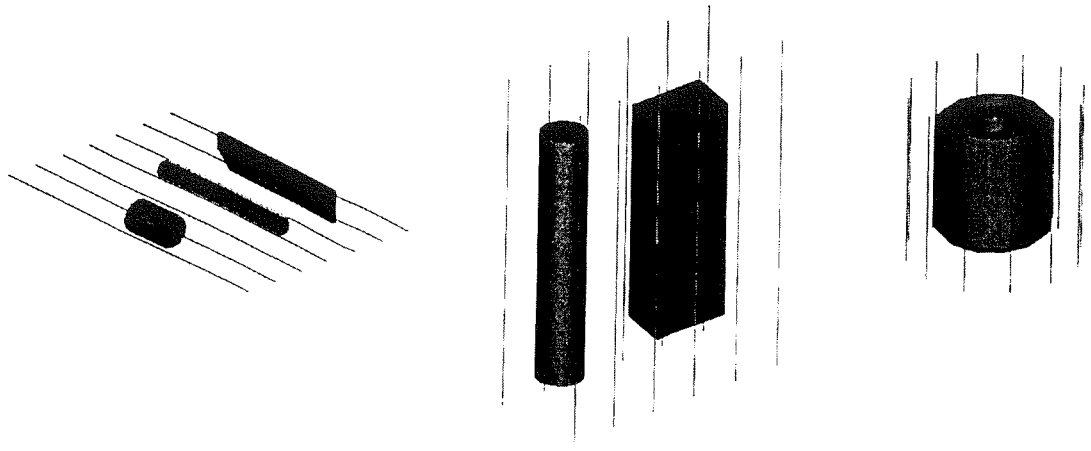

Fig. 5. Model of filament arrays for the production of specially shaped three-dimensional electrodes.

graphitic substrates (Fig. 6) by a large-area HF-CVD process as demonstrated by Fryda, Hampel, Hermann, Schäfer and Klages (1999a) (Fig. 7).

Metallic substrates were pretreated by sand blasting, followed by a cleaning process. The seeding is achieved in an ultrasonic bath containing diamond powder suspended in alcohol. A final cleaning with ultra-pure water follows. Graphite substrates were electroplated with a thin (10–50 nm) Au or Pt interlayer and afterwards seeded and cleaned like the metallic substrates. These electrode substrates were coated with 1–10 μm thick diamond films. Silicon substrates (p-type, 1–10 mΩ cm, semiconductor grade polished) were seeded in the same way as metallic substrates cleaned and coated with a 100–1000 nm thick diamond film. This coating yields a very smooth (50–100 nm roughness), dense and highly conformal, BDD or NBDD coating.

In the HF-CVD unit in Figure 7 (bottom) metallic- and ceramic-based diamond electrodes are usually placed horizontally. For applications where solid dust contamination must be avoided the silicon substrates are placed vertically in the coating unit as shown in Figure 7 (top). This is especially necessary, if the diamond-coated silicon based electrodes of 2–5 in. diameter have to return to

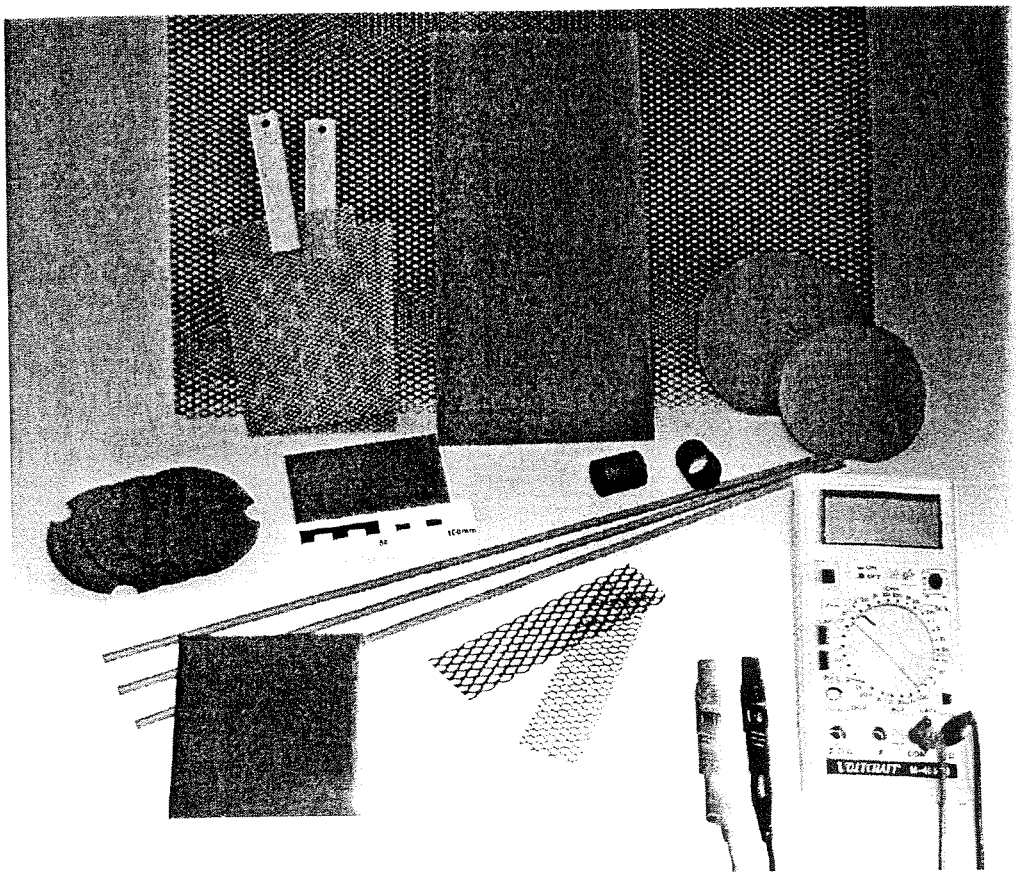

FIG. 6. Boron-doped diamond mesh, plate, tube and cylinder electrodes on tantalum, niobium and graphite base materials.

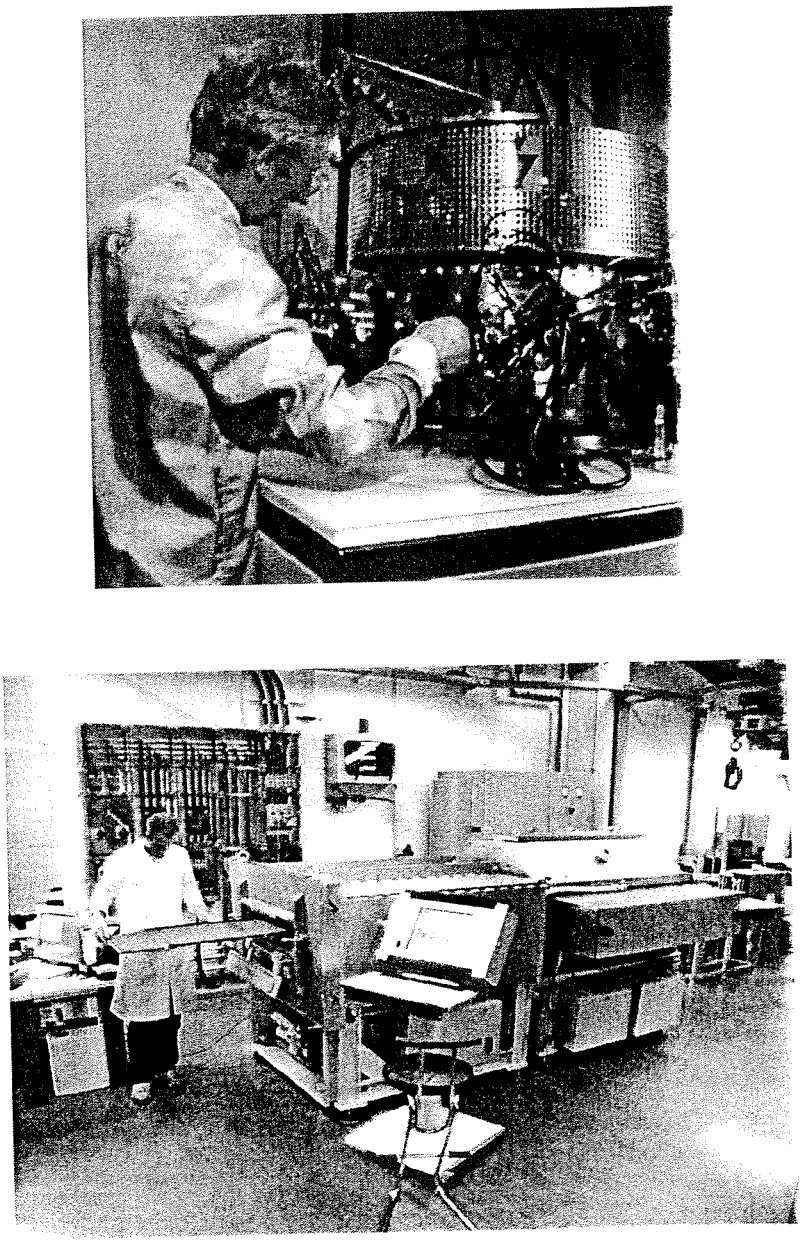

FIG. 7. HF-CVD production plants at CSEM, Switzerland, and Fraunhofer-IST, Germany, for large-area BDD electrodes with coating areas of 6 × ″ (top) and 50 cm × 100 cm (bottom).

the microtechnical process line (clean room class 100) as indicated by Perret et al. (1997).

Before starting a process, the chamber (Fig. 7) with volumes of 0.2–0.75 m^3 was evacuated to a basic pressure of less than 0.1 mbar.

The parameters for the deposition step (heating, deposition and cooling) are the following:

- Filament temperature (2200–2600 °C measured with an optical pyrometer)
- Pressure (10–50 mbar)
- Gas flow (flow rates of 1000–5000 sccm of 0.5–2.5% CH_4 in H_2, 10–200 ppm diborane, for the B/N doped diamond films several % of N_2)

- Substrate temperature (700–925 °C measured by a thermocouple in a dummy substrate) was reproducibly and reliably adjusted and automatically controlled using a programmable process control unit
- These deposition conditions yield typical growth rates of 0.2–2 $\mu m\ h^{-1}$ and boron concentrations in the film of 500–8000 ppm.

After the growth step, the diamond electrodes were slowly cooled to room temperature under pure hydrogen gas.

Conductive-doped diamond layers (resistivities down to 0.005 Ω cm) were deposited directly on Nb, Ta and W with sufficient adhesion for electrochemical applications.

For diamond deposition on Ti, a widely used anode material in industrial electrochemistry, special adaptations are required in order to get sufficient adhesion. On the one hand, the embrittlement and phase transformation of the titanium by hydrogen diffusion must be prevented. On the other hand, stresses at the interface originating from the different thermal expansion coefficients according to the findings of these workers (Heinrich, Grögler, Rosiwal, Singer, Stöckel and Ley, 1996; Andrezza, De Barros, Andrezza-Vignolle, Rats and Vandenbulcke, 1998) must be accommodated.

By a defined surface roughening and the formation of a conducting carbide layer at the interface, sufficient adhesion improvement could be achieved. Diamond can directly be deposited on a polished silicon with good adhesion without special pretreatment.

For quality control each electrode is characterized by light microscope examination and electrical measurement. Sample electrodes of each deposition are also investigated by SEM and cyclovoltammograms in sulfuric acid.

Typical SEM images of metal/diamond electrode surfaces are shown in Figure 8. The visible roughness of several μm is a result of surface roughening pretreatment of the metallic substrate surfaces. The grain size is in the order of 1 μm. The surface morphology changes with increasing boron content in the diamond films.

For electrochemical use all diamond electrodes were anodically polarized in 1 M H_2SO_4 by current densities of 50 mA cm^{-2} for at least 30 min to ensure stable and reproducible conditions.

2.2. Characterization, Testing and Quality Control

Diamond electrodes are a new product for new markets. It is therefore important that the electrodes undergo a rigorous quality control. It is important to gather sufficient statistical data and to establish a product guarantee.

The quality control of diamond electrode production may be executed by non-destructive as well as by destructive testing methods.

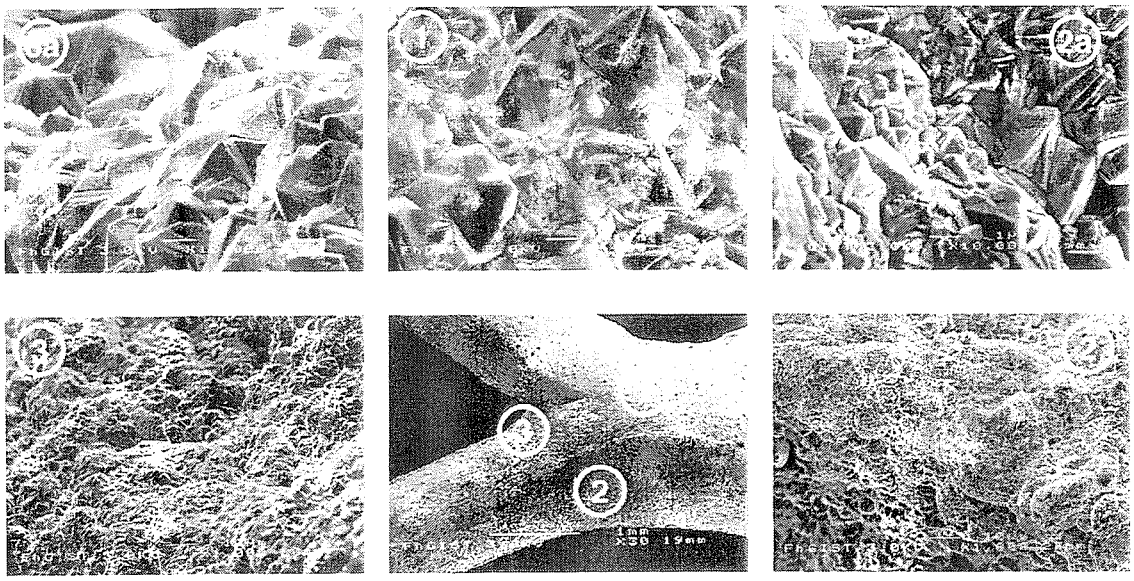

FIG. 8. SEM photographs of diamond film morphology from different areas of a mesh electrode. The continuous diamond film and good crystallinity even in critical zones of the mesh electrode are clearly visible.

Non-destructive testing methods:

1. Visual control of the diamond electrode. Gives a first indication about the quality of the coating.
2. Weight increase and difference. This allows sharing of statistical data concerning reproducibility and reliability of the diamond deposition process as well as the stability of the coating thickness.
3. Scanning electron microscopy (SEM). The SEM control gives a picture of the surface quality of the diamond coatings. Whereas the crystallinity character, shape, distribution and dimensions can well be established, only superficial information can be obtained about pinholes.
4. Raman spectroscopy (RS). RS measurements provide an indication of the sp^2 content in the diamond coating, a factor that is related to the anodic stability of the diamond electrode.
5. Diamond film thickness by any convenient physical film thickness testing method.
6. Local electrochemical testing of the diamond coating by the help of an 'electrochemical pen'.

Destructive testing methods:

1. Bending- and/or fracture probe. Gives a semi-objective indication concerning the adhesion of the diamond coating. This probe can be followed by SEM observation to establish values of layer thickness and layer thickness distribution.
2. Diamond film thickness by calo-wear test or metallographic preparation.

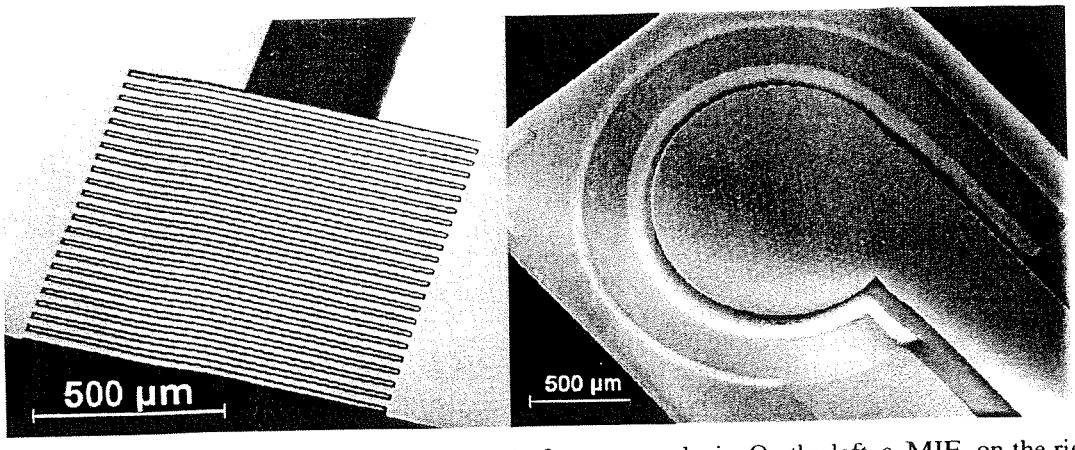

FIG. 9. Two typical shapes of a microelectrode for trace analysis. On the left, a MIE, on the right, parts of a MDA.

Both types of microelectrodes are fabricated using a 4–5 in. Si-wafer support overcoated with silicon oxide/silicon nitride. On this substrate a BDD or NBDD film of 200–800 nm thickness is applied. The conducting diamond film is patterned by reactive ion etching (RIE) and then overcoated with an insulating film of silicon nitride or diamond-like carbon (DLC). This insulating film is itself patterned. Finally, the devices are metallized with Ti/Au or Ti/Al and also patterned (Fig. 10). The devices are sawed out and glued on printed circuit boards (PCB), bonded and sealed with polyepoxid.

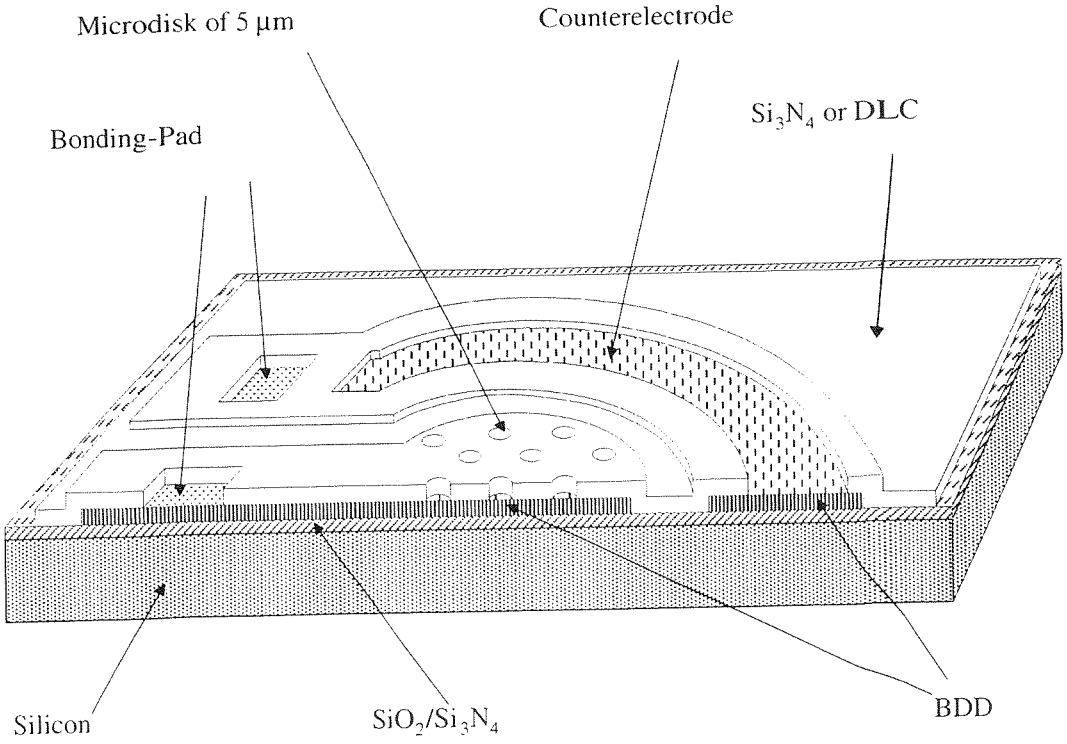

FIG. 10. Schematic structure of a BDD micro-disk array with integrated counter electrode.

The MDA is built of 200 microdisks of 2 or 5 μm in diameter. The counter-electrode, also diamond, surrounds the microdisk array-working electrode. The MDA electrodes are used typically for trace metal analysis of Pb, Cd, Zn, Ag, Cu and Ni. By in-line direct measurement in drinking water 10 $\mu g\, l^{-1}$ (10 ppb) of Ag^+ can be detected. By differential pulse anodic stripping voltammetry 100 ng l^{-1} (100 ppt) of Pb and 50 ng l^{-1} (50 ppt) of Cd could be detected by the workers (Ramesham, 1999a; Madore, Duret, Haenni and Perret, 2000; Rychen, Gobet and Madore, 2001).

The electrode distance in the MIE can be selected from 2 to 10 μm. Interdigitated electrodes can be built in parallel or in conical shape as can be seen in Figure 9. These electrodes are used for the detection of traces of organic molecules as indicated by the workers (Jiali et al., 1996) or for COD measurements by redox reactions.

3.3. Electrodes for Electric Field Measurements in Geophysical Environments

Variations of the electric field have become a subject of intense activity in geophysical research. Long-period magneto-telluric signals are used to probe the lithosphere or the upper mantle conductivity. The spontaneous electric polarization has been observed to be associated with volcanic activity and variations have been observed before earthquakes.

The main problem in measuring electrical potentials in the geophysical environment is the creation of large electrochemical potentials between an electronic or metallic conductor, such as the copper wire going to the recording device, and an electrolytic conductor, such as soil or seawater. The Garchy electrode experiment in 1995/96 from the findings of these workers (Perrier, Petiau, Clerc, Bogorodsky, Erkul, Jouniaux, Lesmes, Macnae, Meunier, Morgan, Nascimento, Oettinger, Schwarz, Toh, Valiant, Vozoff and Yazici-Cakin, 1997) showed that the Ag/AgCl- and the $Pb/PbCl_2$-electrodes are the most convenient electrodes for these measurements.

Short- and long-period magneto-telluric measurements with diamond-disk electrodes of 15 mm in diameter compared with 'standard' Ag/AgCl-electrodes are going on in Switzerland and Germany (Gurk, 2001). The main problem of the first diamond electrodes was their drift over a period of about 24 h (Fig. 11). Surprising was the high sensitivity of these diamond electrodes. The ordinary magneto-telluric distance of electrodes is 50 m, in the case of the diamond electrodes it was 2 m. Even at this small distance the diamond electrodes registered telluric changes.

The initial drift of diamond electrodes could be reduced by an anodic pretreatment with oxygen evolution. A potential difference of ± 5 mV still remains but holds stable. Measurements in the medium periodic band of 2 s show that diamond electrodes remain near to the zero whereas Ag/AgCl-electrodes show drift.

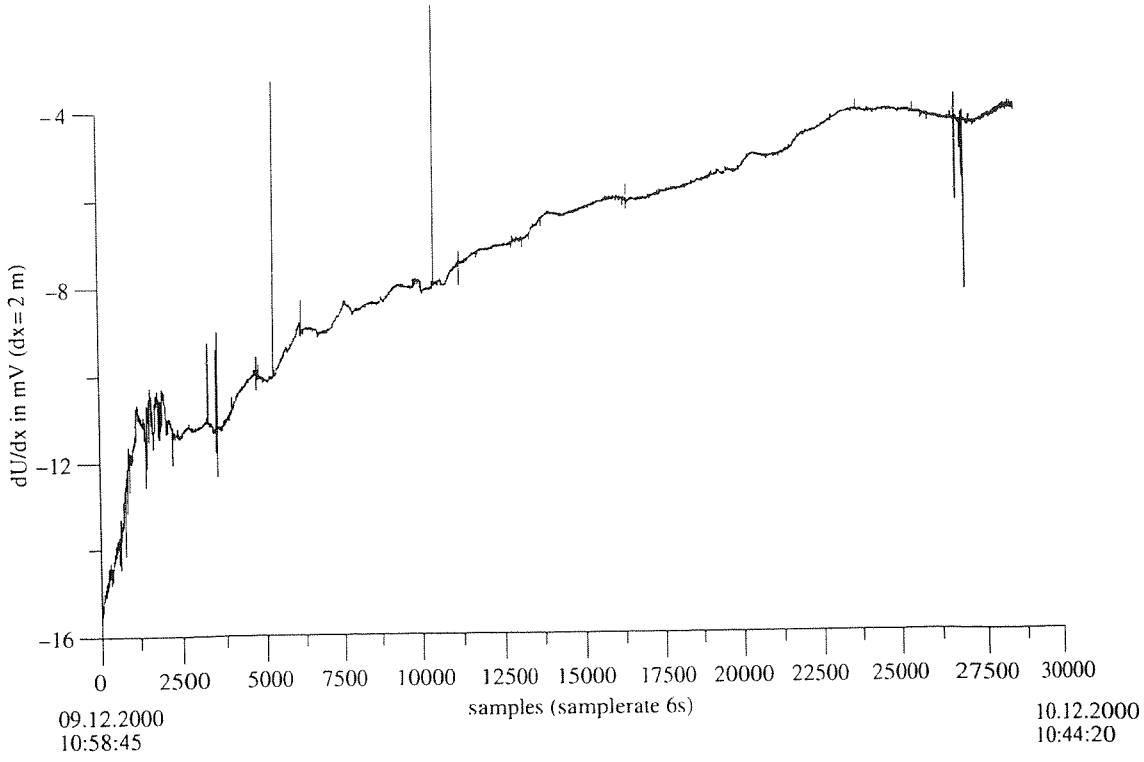

FIG. 11. Magneto-telluric measurements as deposited with diamond electrodes.

4. Electrochemical Reactors for Synthesis and Water Treatment

4.1. INTRODUCTION

Today possible designs of electrochemical reactors using diamond electrodes are limited due to the very directive diamond deposition process and the relatively restricted choice of convenient electrode supporting materials. The deposition process permits only the coating of flat-shaped electrode supports (diameter/high $\geq$ 100), i.e., sheets, grids (mesh), rods, tubes and beads.

All other geometrical forms of electrodes like porous materials cannot be coated. Indeed, a CVI process (chemical-vapor-infiltration) for diamond is up to now not available. Diamond is deposited inside of porous materials with an increasing amount of sp^2 carbon (graphitic or amorphous carbon forms).

A selection of possible electrochemical reactors designed for diamond electrodes is presented in Figure 12.

4.2. MONOPOLAR MESH REACTOR

For the treatment of industrial cycle water GERUS GmbH in Berlin, Germany, developed a monopolar tube reactor (Fig. 13) using a BDD deposited on metallic substrate (Nb).

The reactor consists of a plastic tube, an electrode stack with 18 DiaChem® electrodes $8.25 \times 40\ cm^2$ with a total electrode area of $1\ m^2$.

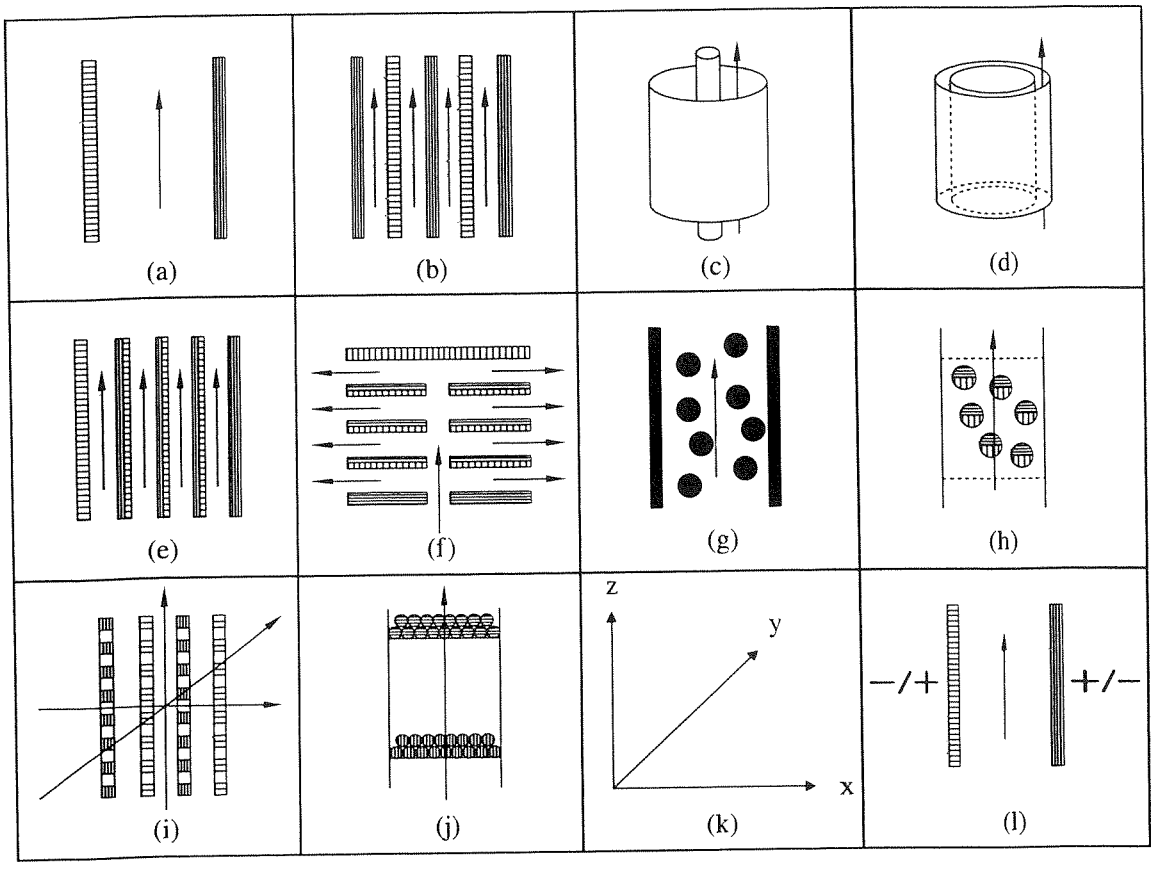

FIG. 12. Basic designs of electrochemical reactors: (a) Monopolar, monocell, plate electrodes, electrolyte flow in z (or y) direction, (b) monopolar, multicell, plateelectrodes, electrolyte flow in z (or y) direction, (c) monopolar, monocell, tube/rod electrodes, electrolyte flow in z direction, (d) monopolar, mono- or multicell, tube electrodes, electrolyte flow in z direction, (e) bipolar, multicell, plate electrodes, electrolyte flow in z (or y) direction, (f) capillary slit, bipolar, multicell, plate electrodes (BASF-type), electrolyte flow: entrance in z direction, exit in x and y direction, (g) three-dimensional bipolar reactor for dynamic bead electrodes with plates, rods or tubes as monopolar electrodes, electrolyte flow in z direction, perpendicular to the electrical field, (h) three-dimensional bipolar reactor for dynamic bead electrodes with porous plate monopolar electrodes, electrolyte flow in z direction parallel to the electric field, (i) monopolar, mono- or multicell, mesh/grid electrodes, electrolyte flow in x, y and z direction, (j) monopolar, mono- or multicell, mesh/grid or static bead electrodes, electrolyte flow in z direction parallel to the electric field, (k) indication of flow direction and (l) possibility of polarity exchange if both electrodes are of diamond.

The distance between the electrodes is 4–5 mm. During electrochemical use a potential of 5–10 V and a current of 150 A is applied. For removal of calcareous deposits formed on the cathodes the polarity is reversed. The pilot plant achieves a COD removal rate of 45 g O_2 h^{-1}.

Depending on the application, such a reactor type could be scaled up as well as scaled down.

4.3. Modular Electrochemical Reactor: DiaCell®

A registered, modular electrochemical cell system, called DiaCell® developed by the workers (Haenni, Faure and Rychen, 2001a), based on circular (100 mm in

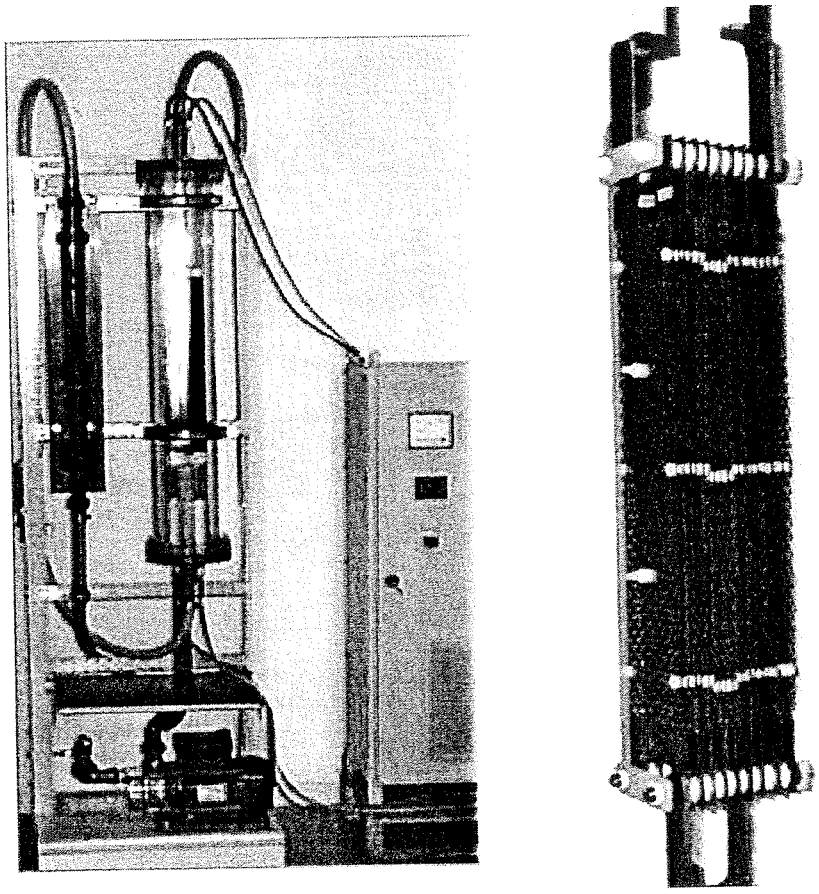

FIG. 13. Pilot plant reactor for the treatment of industrial cycle water from GERUS GmbH in Berlin, Germany (left side) and electrode stack of the pilot plant with 18 diamond electrodes (right side).

diameter) diamond electrodes for ceramic and metallic supports, has been developed for laboratory use and pilot plant applications. All other types of circular electrodes, like DSAs on titanium, glassy-carbon, platinum on titanium, zirconium or nickel can also be mounted in this cell.

Figure 14 shows the basic bipolar electrochemical cell module. On the exploded view the two current feeder electrodes with their housings can be seen in which the liquid entrance, respectively, exit are located. The bipolar electrode is positioned between the two current feeder electrodes. The seals are at the same time liquid distributors through the individual cell compartments.

The DiaCell® allows stack mounting of maximum five cell compartments in bipolar mode. The cell can also function in monopolar mode without or with one or two diaphragms. Each module can be operated with an adjustable electrode distance of 1, 2, 5 or 10 mm. The modules are tight up to 2 bar. A high-pressure module for operation up to 12 bar is in development. The volumetric flow rate of the electrolyte is 200–300 l min^{-1} per compartment with a pressure drop of about 0.3 bar.

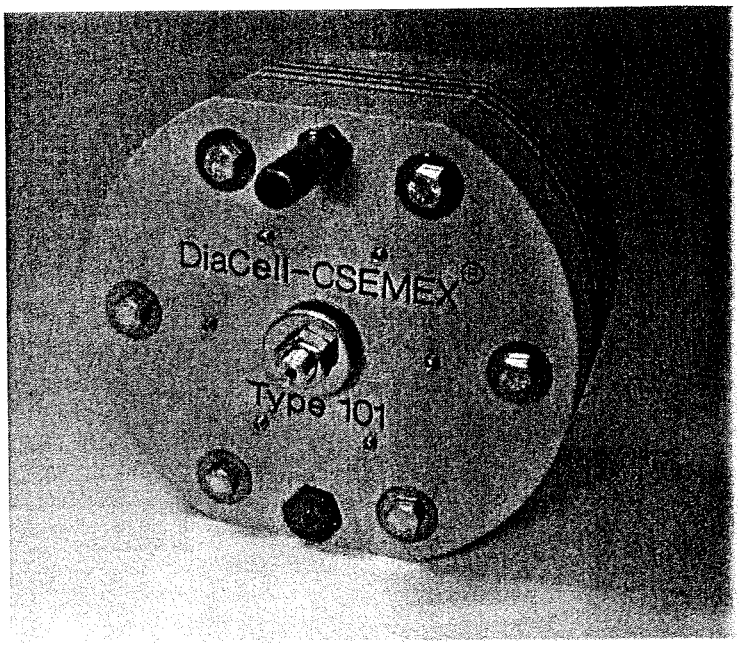

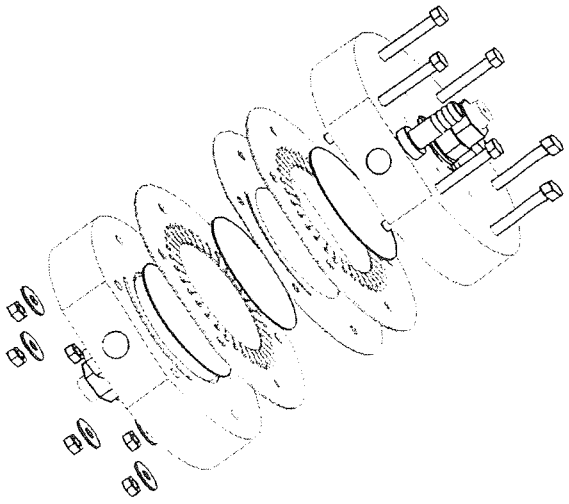

FIG. 14. Top: DiaCell® as used for swimming pool, ballast and waste water treatment and disinfection. The module is equipped with three compartments (two current feeders and two bipolar-electrodes). Inter-electrode distance 10 mm. Bottom: The exploded view of the basic bipolar module of the electrochemical cell system.

The DiaCell® can be driven with a potential of maximum 48 V for non-insulated connection (low) and a current of maximum 150 A. Several cells can be mounted in parallel or in series.

For water disinfection, like swimming pools, ballast water and gray water treatment or fresh water disinfection, the system can be equipped with sensors for the controlled production of chlorine or ozone.

This DiaCell® system is subject to adaptation at any time to future diamond plate electrode dimensions like 100×100, 125×200, 200×250 and $250 \times 400\ mm^2$.

5. Electrosynthesis of Organics and Oxidants

5.1. Introduction

Although much work has been done in organic and inorganic electrosyntheses, few processes have been applied on an industrial scale.

In our opinion the main reason for this is the low electrochemical stability of the available electrode material, especially in acid solutions at high current densities. Electrode deactivation and fouling during operation also causes serious problems.

BDD electrodes have high electrochemical stability; they are not deactivated during operation and furthermore exhibit high overpotential for both oxygen and hydrogen evolution. These properties of BDD can open new possibilities in industrial electrosynthesis.

Hereafter we present results concerning electroorganic synthesis (benzoquinone, nicotinic acid) and electro-inorganic synthesis (production of powerful oxidants) as well as practical and potential applications.

BDD films deposited on p-Si substrate have been used as anode and Zr metal as cathode.

Two types of electrochemical cells (DiaCell®) have been used: a one-compartment or a two-compartment cell. The two-compartment cell (using a Nafion® membrane) was used in some cases to minimize losses in current efficiency induced by the reduction of the oxidized product.

5.2. Electroorganic Synthesis Using BDD Anode

Two examples are given to demonstrate the feasibility of electroorganic synthesis on BDD anodes. The first example is the oxidation of phenol to benzoquinone, an important intermediate in fine organic synthesis. The second example is the oxidation of 3-methylpiridine to nicotinic acid, an important pharmaceutical intermediate. Many other electroorganic syntheses may be possible and exploited in the future as demonstrated by these workers (Pütter, Weiper-Idelmann and Merk, 1999).

Both electrosynthetic processes have been reported previously using classical electrodes like lead dioxide. However, the main problems with these electrodes are the low anodic stability under the operating conditions used and the deactivation of the electrode due to fouling.

BDD electrodes are very stable, even at high anodic potential, and are not prone to fouling. Due to these unique properties, BDD can open new opportunities in electroorganic synthesis.

5.2.1. *Oxidation of Phenol to Benzoquinone*

The electrochemical behavior of phenol in acid medium (1 M $HClO_4$) at BDD electrode has shown following these workers (Iniesta, Michaud, Panizza, Cerisola, Aldaz and Comninellis, 2001a) that:

- In the potential region of water stability the anodic oxidation of phenol results in the deactivation of the electrode due to the formation of polymeric products on the anode surface.
- The electrode can be restored to its initial activity by treatment at high anodic potential.
- The oxidation products of phenol in the potential region of water decomposition depend on the applied current density, phenol concentration and phenol conversion.

In fact, preparative bulk electrolysis of phenol on BDD anodes under galvanostatic conditions has shown that depending on experimental conditions it is possible to obtain partial oxidation of phenol to aromatic compounds or its complete oxidation to CO_2 following the workers (Iniesta et al., 2001a).

In particular, at low-current density and low-phenol conversion, only aromatic compounds (benzoquinone, hydroquinone and catechol) are formed during phenol oxidation.

The electrochemical oxidation of phenols to aromatic compounds on BDD involves certain active intermediates formed by water discharge and hydroxyl radicals (Eq. (1)), which react with phenol (Eq. (2)) in a fast reaction close to the electrode surface.

$$H_2O \rightarrow OH^{\cdot} + e^- + H^+ \tag{1}$$

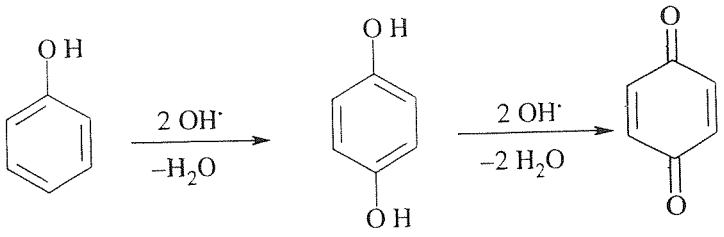

(2)

A typical example of HPLC analysis of the solution during phenol oxidation carried out in the one-compartment DiaCell® cell at low current density (5 mA cm^{-2}) is given in Figure 15.

Under these conditions, and for a low phenol conversion ($X < 20\%$), the concentration of phenol decreases linearly with the specific charge forming mainly benzoquinone with a small amount of hydroquinone and catechol. It is worth noting that the electrode potential remains almost constant during electrolysis (2.5 ± 0.1 V vs. SHE) and there is no indication of electrode deactivation under these conditions.

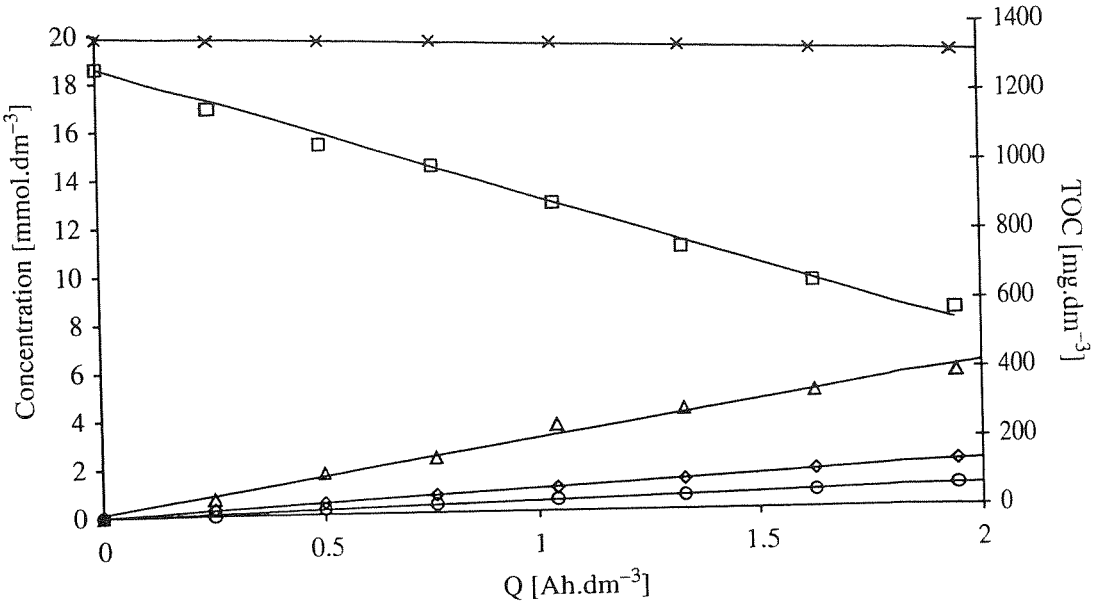

FIG. 15. Concentration trends during phenol electrolysis on BDD anode: (□) phenol, (△) benzoquinone, (◇) hydroquinone, (○) catechol and (×) TOC electrolyte: 1 M $HClO_4$; initial phenol concentration = 20 mM; $T = 25$ °C; $i = 5$ mA cm^{-2}, anode potential $E = 2.5 \pm 0.1$ V vs. SHE. Reprinted with permission from: J. Iniesta, P.-A. Michaud, M. Panizza, G. Gerisola, A. Aldaz, and Ch. Comninellis, *Electrochim. Acta*, In press. Copyright 2001. Elsevier Science Ltd.

In confirmation of the partial oxidation of phenol to aromatic compounds (benzoquinone, hydroquinone and catechol), Figure 15 also shows that the total organic carbon (TOC) in the solution remains almost constant during electrolysis. This indicates that the oxidation of phenol to CO_2 does not occur under these conditions.

5.2.2. *Oxidation of 3-Methylpyridine to Nicotinic Acid*

The anodic behavior of 3-methylpyridine (3-MP) on BDD anode is very similar to the anodic oxidation of phenol, namely found by the workers (Iniesta, Michaud, Panizza and Comninellis, 2001b):

- In the potential region of water stability the anodic oxidation of 3-MP results in the deactivation of the electrode.
- The electrode can be restored to its initial activity by treatment at high anodic potential.
- The oxidation products of 3-MP in the potential region of water decomposition depend on the applied current density and 3-MP conversion.

Bulk electrolysis of 3-MP in 0.5 M $HClO_4$ in a one-compartment DiaCell® cell at low current density (2.5 mA cm^{-2}) and for low 3-MP conversion has shown that partial oxidation of 3-MP to nicotinic acid can be achieved as found by the workers (Iniesta et al., 2001b).

A typical example for the partial oxidation of 3-MP is given in Figure 16. This figure also shows that the TOC of the electrolyte remains almost constant during electrolysis confirming the partial oxidation of 3-MP.

As in the case of phenol oxidation, hydroxyl radicals formed by water discharge on BDD anode (Eq. (1)) participate in the oxidation of 3-MP to nicotinic acid (Eq. (3)):

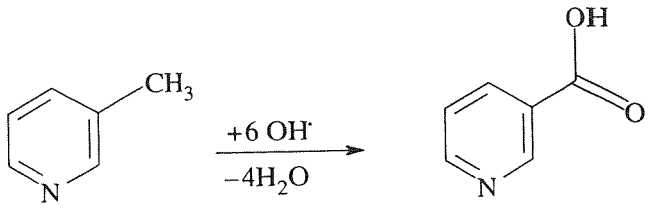

(3)

Furthermore, there is no indication of electrode deactivation during 3-MP oxidation under these experimental conditions.

5.3. Preparation of Powerful Oxidants

The unique properties of BDD electrodes are:

- High anodic stability in strongly acidic media
- High oxygen evolution overpotential due to the slow kinetics of oxygen formation

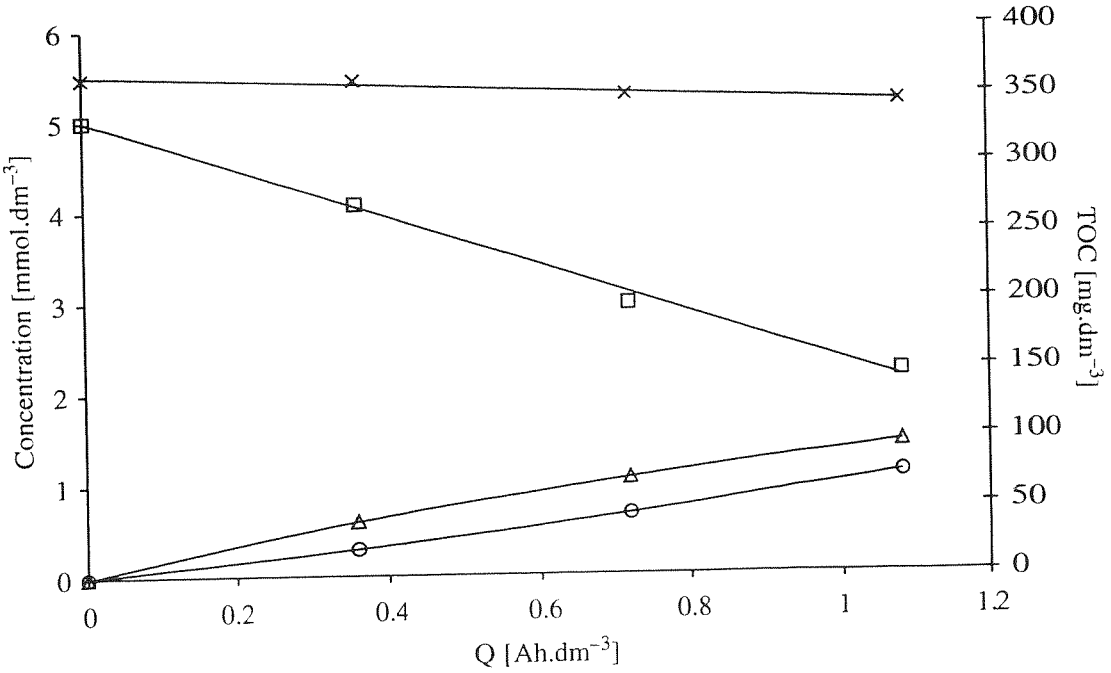

Fig. 16. Concentration trends during 3-MP electrolysis on BDD anode: (□) 3-MP, (△) nicotinic acid, (○) oxidation intermediates and (×) TOC electrolyte: 0.5 M $HClO_4$; initial 3-MP concentration = 5 mM; $T = 25$ °C; $i = 2.5$ mA cm^{-2}, anode potential $E = 2.7 \pm 0.1$ V vs. SHE. Reprinted with permission from: J. Iniesta, P.-A. Michaud, M. Panizza, and Ch. Comninellis, *Electrochem. Commun.* 3, 346 (2001). Copyright 2001. Elsevier science Ltd.

- Formation of active intermediates (hydroxyl radicals) during water discharge.

These characteristics allow the production of powerful oxidants with high redox potential.

We can distinguish two main categories of oxidants:

- Oxidants, which are produced in a 'facile' reaction and are involved in a fast electron transfer reaction independently of the type of anode used.

Typical examples are the following couples:

$$Ce(IV)/Ce(III)\ [E_0 = 1.71\ V]$$

$$Co(III)/Co(II)\ [E_0 = 1.93\ V]$$

$$Ag(II)/Ag(I)\ [E_0 = 1.98\ V\ vs.\ SHE].$$

- Oxidants, which are produced in a 'demanding' reaction and are produced indirectly via hydroxyl radicals generated by water discharge according to the findings of the workers (Comninellis, Michaud, Haenni, Perret and Fryda, 1999; Panizza et al., 2000a,b).

Typical examples are the following couples:

$$Cr_2O_7^{-2}/Cr^{+3}\ [E_0 = 1.36\ V]$$

$$H_2O_2/H_2O\ [E_0 = 1.76\ V]$$

$$S_2O_8^{-2}/SO_4^{-2}\ [E_0 = 2.0\ V\ vs.\ SHE].$$

One example for each category is treated below. The 'facile' reaction of Ag(I) oxidation to Ag(II) and the 'demanding' reaction of sulfate to peroxodisulfate oxidation:

- The Ag(I)/Ag(II) couple can be used as mediator in the electrochemical oxidation for synthesis, and for the treatment of nuclear wastes.
- Of the many applications of peroxodisulfate, the two most important are in etching printed circuits and in acrylonitrile polymerization. Other applications are wastewater treatment, dye oxidation and fiber whitening.

5.3.1. Oxidation of Ag(I) to Ag(II) in Concentrated HNO_3

Silver (II) is well known for being a strong oxidant in acidic media ($E_0 = 1.98$ V vs. SHE). One attractive method for Ag(II) production is the

electrochemical oxidation of Ag(I) in concentrated HNO_3 (Eq. (4)).

$$Ag(I) \rightarrow Ag(II) + e^- \quad (4)$$

The anodic oxidation of Ag(I) to Ag(II) can be performed on platinum, gold and antimony-doped SnO_2 electrodes. However, these electrodes suffer from limited anodic stability in concentrated HNO_3 and low current efficiency for Ag(II) formation.

Figure 17 shows typical cyclic voltammetric curves for BDD in 10 M HNO_3 in the presence of different concentrations of Ag(I). In the absence of Ag(I) (curve a), the voltammogram shows that the anodic current density starts to increase only above 2.1 V vs. SHE mainly due to the oxygen evolution reaction following these workers (Panizza et al., 2000a,b).

In presence of Ag(I) (curves b–f), an anodic current peak was observed at approximately 2.2 V vs. SHE. This peak corresponds to the oxidation of Ag(I) to Ag(II) according to Eq. (4). The current oxidation peak maximum is directly proportional to Ag(I) concentration (Fig. 17 inset) (Panizza et al., 2000a,b).

The diffusion coefficient of Ag(I) in 10 M HNO_3 was calculated from the slope of the straight line in Figure 17 inset, to give $D = 8.51 \times 10^{-6}$ cm^2 s^{-1}, using Randles-Sevcik equations. This value is close to the values given in the literature.

The cyclic voltammetric curves also show large and insignificantly defined peaks for the reduction of silver (II) at about 1.2 V vs. SHE.

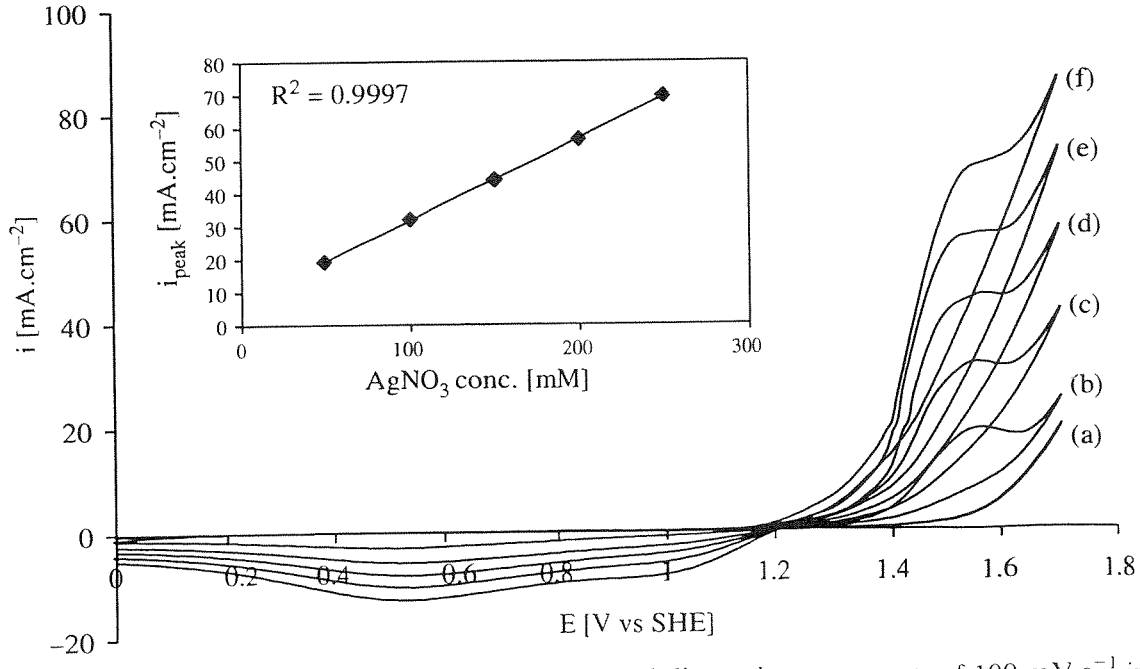

FIG. 17. Cyclic voltammetric behavior of boron-doped diamond at a scan rate of 100 mV s^{-1} in 10 M HNO_3 with different Ag(I) concentrations (mM): (a) 0, (b) 50, (c) 100, (d) 150, (e) 200 and (f) 250. The dependence of the peak current density on the Ag(I) concentration is shown in the inset. Reprinted with permission from: M. Panizza, I. Duo, P.-A. Michaud, G. Gerisola, and Ch. Comninellis, *Electrochem. Solid-State Lett.* 3 (12), 550 (2000). Copyright 2001. The Electrochemical Society Inc.

From the comparison of the voltammograms in the presence and absence of silver (I), we can predict that silver (II) can be produced with high-current efficiency by oxidation of silver (I) at BDD anodes under potentiostatic conditions at 2.2 V vs. SHE. In fact, preparative electrolysis in a solution of 10 M HNO_3 + 100 mM $AgNO_3$, applying a constant potential of 2.2 V vs. SHE results in 11% conversion of Ag(I) to Ag(II) after 2 h of electrolysis with a current efficiency of 81% (Panizza et al., 2000a,b).

5.3.2. *Oxidation of Sulfate to Peroxodisulfate*

Peroxodisulfuric acid $H_2S_2O_8$, and its salts are among the strongest known oxidizing agents (E_0 = 2.01 V vs. SHE):

$$2SO_4^{-2} \rightarrow S_2O_8^{-2} + 2e^- \tag{5}$$

The efficiency of the electrochemical production of peroxodisulfate strongly depends on the electrode material. High oxygen overpotential anodes must be used to minimize the side reaction of oxygen evolution. The conventional electrochemical process for peroxodisulfate synthesis uses smooth platinum anodes.

Main problems in the peroxodisulfate production process using Pt anode are: high corrosion rate of Pt, additives used (thiocynates), purification of the electrolyte before recycling from the corrosion product of the Pt and from the additives.

Preparative electrolysis has been carried out in a two-compartment DiaCell® electrolytic flow cell under galvanostatic conditions. During electrolysis the main side reaction is the anodic oxygen evolution (Eq. (6))

$$2H_2O \rightarrow O_2 + 4H^+ + 4e^- \tag{6}$$

and the chemical decomposition of peroxodisulfate to O_2 (Eq. (7)) to monopersulfate (Eq. (8)), which is further decomposed to H_2O_2 (Eq. (9))

$$S_2O_8^{-2} + H_2O \rightarrow 2HSO_4^- + \tfrac{1}{2}O_2 \tag{7}$$

$$S_2O_8^{-2} + H_2O \rightarrow SO_5^{-2} + SO_4^{-2} + 2H^+ \tag{8}$$

$$SO_5^{-2} + H_2O \rightarrow H_2O_2 + SO_4^{-2} \tag{9}$$

In order to find the optimal conditions of peroxodisulfate formation on BDD, the influence of operating conditions (T, H_2SO_4 concentration) on the current efficiency of peroxodisulfate formation as investigated by the workers (Michaud, Mahé, Haenni, Perret and Comninellis, 2000).

Figure 18 shows the influence of H_2SO_4 concentration on the current efficiency of peroxodisulfate formation.

At low H_2SO_4 concentration (< 0.5 M) the main side reaction is the discharge of water to O_2 (Eq. (6)). The chemical decomposition of peroxodisulfate (Eqs. (7)–(9)) also takes place at this low H_2SO_4 concentration.

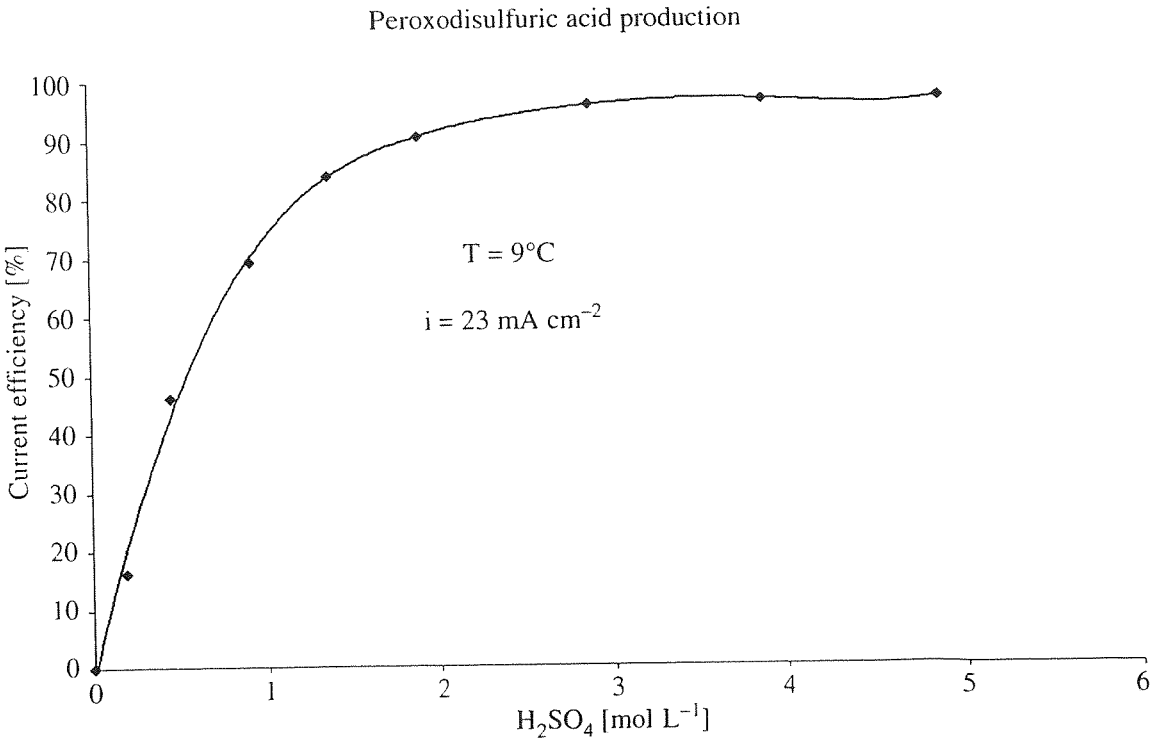

FIG. 18. Current efficiency of peroxodisulfate formation vs. the H_2SO_4 concentration.

At high H_2SO_4 concentration (>2.0 M) the main anodic reaction is the electrochemical oxidation of sulfate to peroxodisulfate (Eq. (5)). Small amounts of monopersulfate (Eq. (8)) and H_2O_2 (Eq. (9)) are also formed by the chemical decomposition of peroxodisulfate.

Figure 19 shows the influence of the temperature on the current efficiency of peroxodisulfate formation in 1 M H_2SO_4 under galvanostatic conditions (23 mA cm^{-2}).

The decrease of current efficiency with the temperature is due to the chemical decomposition of peroxodisulfate to oxygen (Eq. (7)).

The workers (Comninellis et al., 1999; Michaud et al., 2000) speculate that hydroxyl radicals are involved in the electrochemical oxidation of sulfate to peroxodisulfate.

According to this mechanism, hydroxyl radicals formed by water discharge (Eq. (1)) react with HSO_4^- (which is the main species in conc. H_2SO_4), giving peroxodisulfate (Eq. (10)):

$$2HSO_4^- + 2OH^{\cdot} \rightarrow S_2O_8^{-2} + 2H_2O \qquad (10)$$

BDD electrodes on metallic and silicon substrates have also been tested on industrial sites, e.g., for ammonium peroxodisulfate production by Lehmann (2000a,b). Figure 20 shows the economic advantage of BDD electrodes against platinum electrodes. Reduced current densities at diamond electrodes allow substantial reduction of electrical energy consumption at comparable high electrode area production capacity.

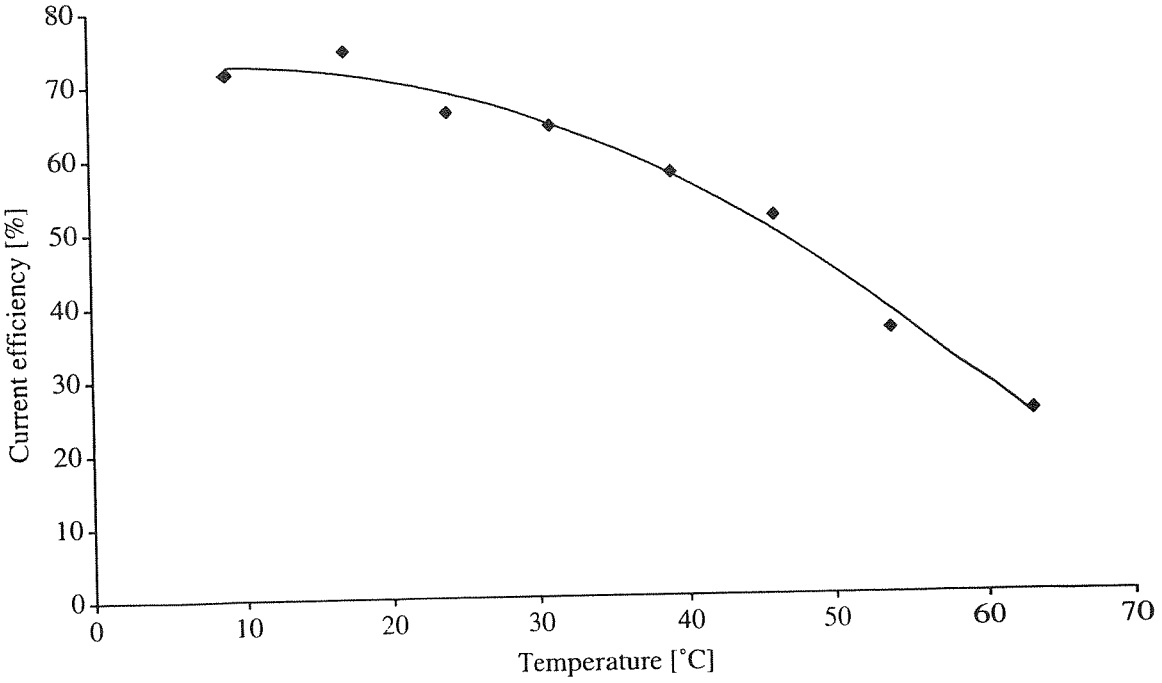

FIG. 19. Influence of temperature on the current efficiency of peroxodisulfate formation in 1 M H_2SO_4, on BDD anode, $i = 23$ mA cm^{-2} H_2SO_4 conversion: 5%.

5.4. OTHER POTENTIAL APPLICATIONS

As indicated in the introduction to Section 5.3 there are other oxidants that have been studied and produced:

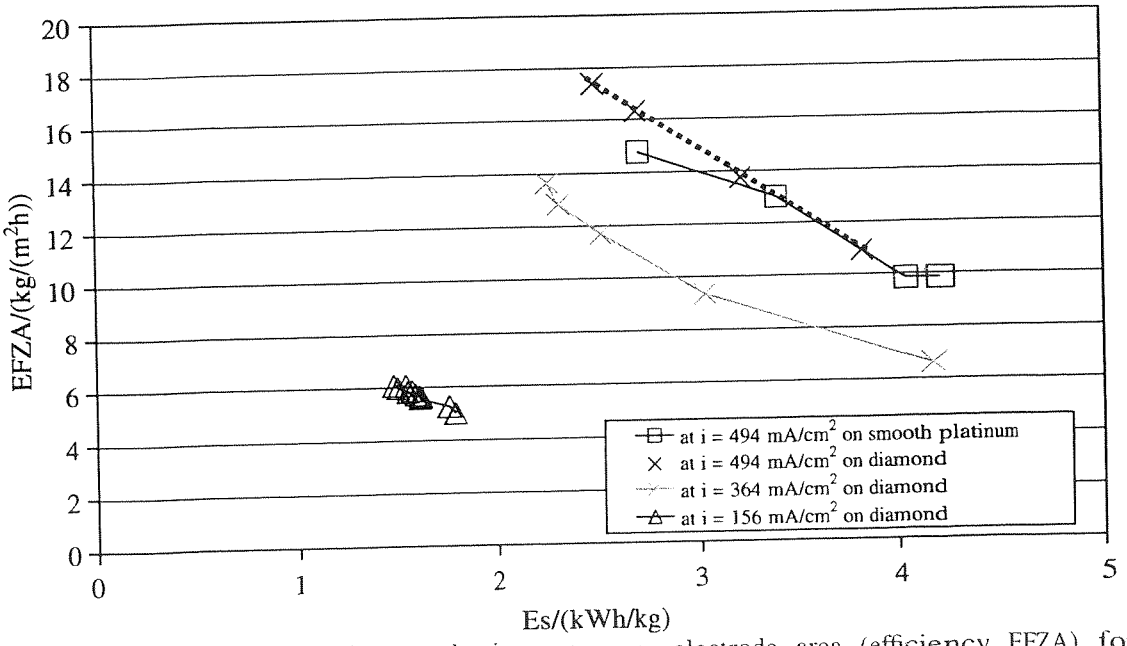

FIG. 20. Ammonium persulfate production rates per electrode area (efficiency EFZA) for different energy consumption levels per produced mass (Es) compared with diamond and platinum electrodes.

- Chlorine/hypochloride (Ferro, De Battisti, Duo, Comninellis, Haenni and Perret, 2000; Kraft, Stadelmann and Kirstein, 2000; Lorenz, Pupunat, Comninellis, Correa, Haenni and Perret, 2000)
- Ozone (Perret et al., 1997; Swain, Anderson and Angus, 1998; Wurm, Fryda and Schäfer, 1999).
- $Cr_2O_7^{-2}/Cr^{+3}$ (Iniesta et al., 2001a,b).

5.4.1. *Chlorine/Hypochloride*

Unfortunately, the electrochemical synthesis of hypochlorides and chlorine on conventional electrodes (platinum, DSA®) is still not well understood. The production of hypochlorides and chlorine on diamond is even increasing the confusion. In some cases (Ferro et al., 2000; Kraft et al., 2000; Lorenz et al., 2000), the production of chlorine is more efficient than with DSA or Pt. Under slightly different conditions the chlorine production may be considerably less than on DSAs. It is possible that on diamond electrodes a concurrent production of other even more powerful oxidants like ozone and hydrogen peroxides occurs. More investigations must be performed on this matter.

5.4.2. *Ozone*

The authors (Perret et al., 1997; Swain et al., 1998) mentioned the ozone production in sulfuric acid and in fluoridic media on BDD electrodes. Ozone can also be produced with an interesting yield in ultra-pure water in a solid polymer membrane cell as well as during water treatment and disinfection with BDD electrodes following the findings of workers (Wurm et al., 1999; Lorenz et al., 2000).

5.4.3. *Galvanic Applications*

Diamond-coated titanium and niobium electrodes provide unique advantages for industrial electrochemical processes. The overpotential for oxygen evolution in water containing electrolytes is in the region of 2.7–2.9 V, which is much higher than conventional electrode materials, e.g., lead or mixed metal oxide (MMO) electrodes. This advantage offers the possibility of using diamond electrodes efficiently for several processes in the electroplating industry.

DiaChem® electrodes with different geometries and dimensions were produced using large-area HF-CVD. The typical diamond film thickness is between 2 and 5 μm. Doping levels of a few thousand ppm boron yield electrical resistivities lower than 50 mΩ cm.

For lifetime tests these DiaChem® electrodes have been loaded with increasing current densities up to 4 A cm^{-2} in sulfuric acid over months. Degradation of the electrode surface or the electrochemical performance could not be detected, thus demonstrating the extreme chemical stability of these electrodes.

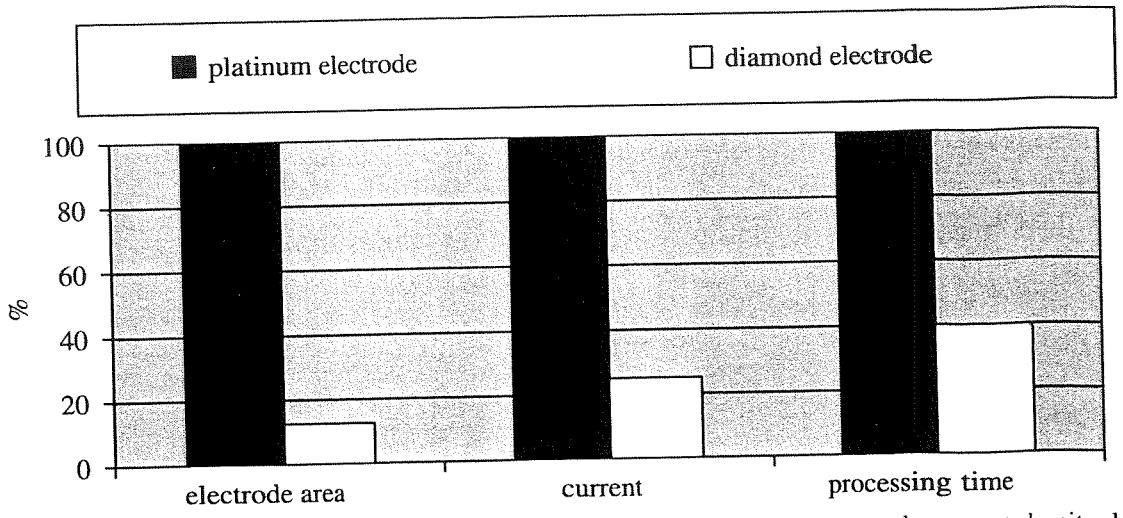

FIG. 21. Increase of electrode efficiency by reduction of electrode area and current density by applying DiaChem® electrodes for the oxidation of Cr^{III} to Cr^{VI} in chromic sulfuric acid for etching ABS plastics.

For galvanic applications DiaChem® electrodes have been tested in the production environment of electroplating industry. Examples of these applications have been demonstrated by the workers (Iniesta et al., 2001b, Wurm, 2001):

- Oxidation anode in combination with MMO electrodes as working electrodes in a 'lead-free' chromium electroplating process
- Oxidation of Cr^{III} to Cr^{VI} in chromic sulfuric acid for etching ABS plastics
- Decomposition of organic or cyanide additives in electroplating baths.

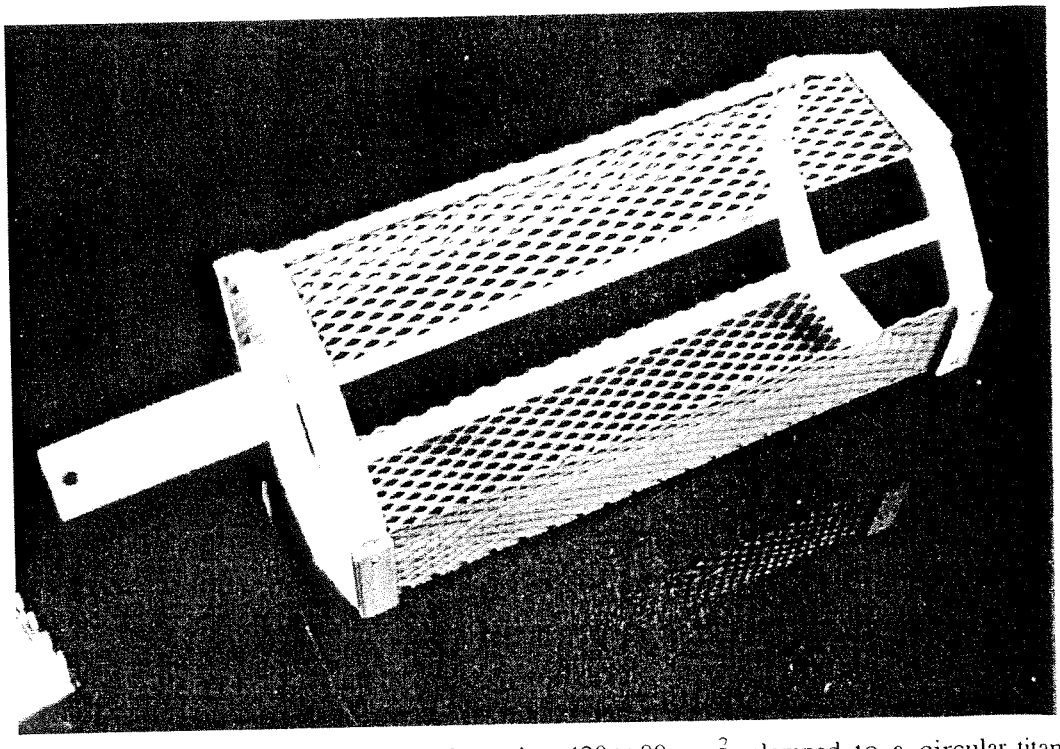

FIG. 22. Diamond coated niobium meshes, size $420 \times 80\ mm^2$, clamped to a circular titanium frame for Cr^{III} to Cr^{VI} oxidation.

Compared with the well-known oxidation of Cr^{III} with Pt/Ti anodes in a chromic acid/sulphuric acid etching mixture for ABS plastics, the diamond-coated surface could be reduced to 1/8 of the platinum-coated surface area and works with only 1/4 of the current (Fig. 21). The efficiency for this process with DiaChem® electrodes is excellent and therefore allows the replacement of the installation by a much smaller unit. The anode used for this task is shown in Figure 22.

6. Application of BDD Electrodes in Water Treatment

6.1. Introduction

Many organic and inorganic pollutants containing wastewaters are produced by industry. These wastewaters must be treated by physical, chemical or biological methods before discharge.

Recently, electrochemical water treatment has been proposed. However, the major problem with this process is to find an adequate anode material. The BDD electrodes, which have high electrochemical stability and a large potential window, open new possibilities for water treatment.

Three examples for the treatment of wastewater are presented here: the electrochemical treatment of water containing toxic and organic pollutants, the treatment of wastewater containing cyanides and the disinfection of swimming pool water.

BDD films deposited on p-Si substrate have been used as anode and Zr as cathode in a one-compartment DiaCell® electrochemical cell.

The distance between electrodes in this cell is 10 mm. The electrolyte is recirculated through the cell and a glass reservoir ($V = 500$ ml) using a centrifugal pump (Fig. 23).

6.2. Electrochemical Treating of Waste Water Containing Organic Pollutants

Biological treatment of polluted water is the most economical process and is used for the elimination of 'readily degradable' organics present in wastewater. The situation is completely different when the wastewater contains refractory (resistant to biological treatment) organic pollutants or if their concentration is high and/or very variable. In this case, another type of treatment must be used.

Many treatment technologies are already in use or have been proposed for the recovery or destruction of pollutants. These technologies include activated carbon adsorption and solvent extraction for recovery or oxidation for destruction. Several applications of chemical oxidation using hydrogen peroxide and ozone have been reported.

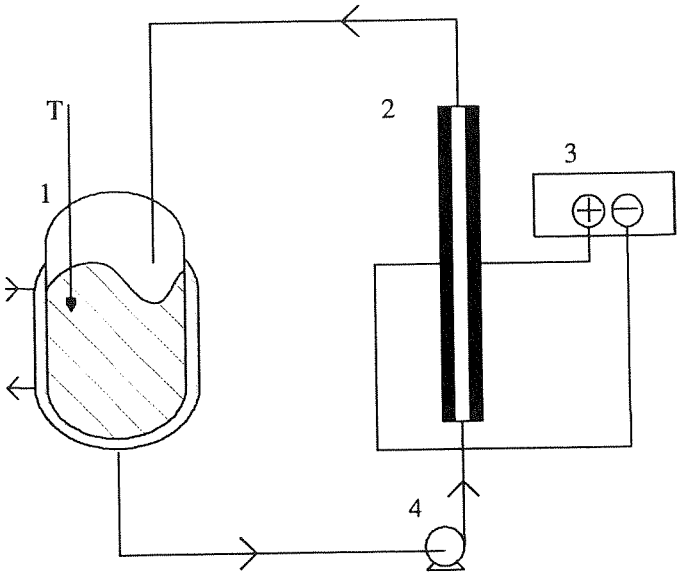

FIG. 23. Set-up used for electrochemical wastewater treatment using BDD anodes: 1: 500 ml reservoir, 2: DiaCell® electrochemical cell, 3: power supply and 4: recirculation pump.

The electrochemical method for the treatment of wastewater containing organic pollutants has attracted a great deal of attention recently. Major advantages are the ease of control and increased efficiencies. Another advantage is the possibility of building compact bipolar electrochemical reactors.

The aim of the present work was to investigate the anodic oxidation of some model organic pollutants at BDD anodes to examine the reaction mechanism and to elucidate the possibilities of the electrochemical method for wastewater treatment.

Mechanism of the anodic oxidation of organics: Two mechanisms can be distinguished for the electrochemical oxidation of organic compounds: direct oxidation and indirect oxidation via electro-generated intermediates formed at the anode surface.

Cyclic voltammetry has been used to investigate the mechanism of the electrochemical oxidation of two classes of organic compounds on BDD:

- simple carboxylic acids (formic, oxalic and acetic acid),
- phenolic compounds (phenol, chlorophenol and β-naphtol).

6.2.1. Oxidation of Carboxylic Acids on BDD

The decomposition behavior of carboxylic acids was determined by cyclic voltammography in 1 M H_2SO_4 at 25 °C containing different concentrations of the organic acids. For all carboxylic acids examined the cyclic voltammograms, i.e., in Figures 24 and 25, the decomposition potential of water/electrolyte displays no significant change in the presence of organic acids compared to the voltammogram of the pure electrolyte. The only difference in

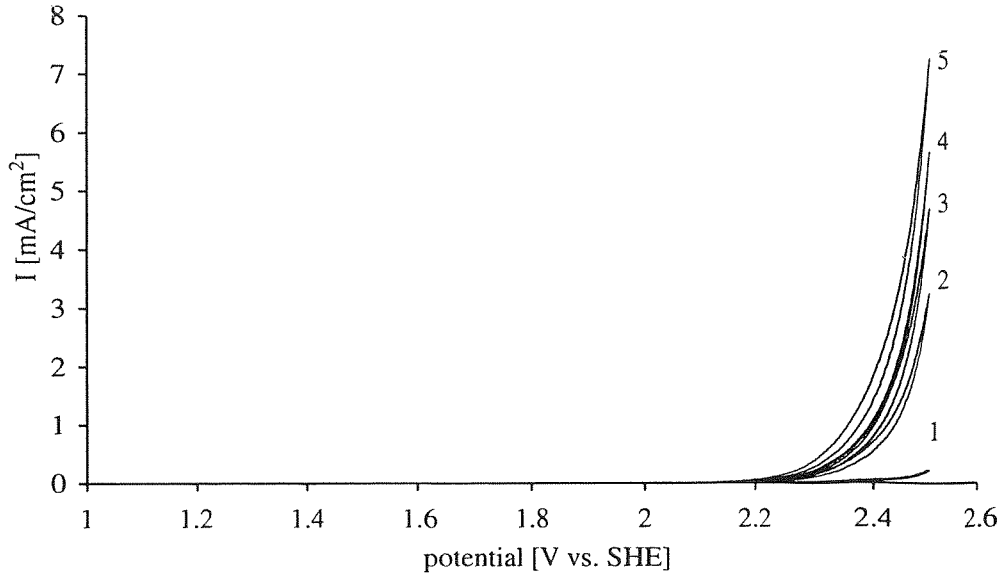

FIG. 24. Cyclovoltammograms of BDD (1) in 1 M H_2SO_4, (2) in 1 M H_2SO_4 + 0.05 M formic acid, (3) in 1 M H_2SO_4 + 0.1 M formic acid, (4) in 1 M H_2SO_4 + 0.2 M formic acid and (5) in 1 M H_2SO_4 + 0.5 M formic acid. Scan rate: 50 mV s^{-1}, $T = 25$ °C. Reprinted with permission from: D. Gandini, E. Mahé, P.-A. Michaud, W. Haenni, A. Perret, and Ch. Comninellis, *J. Appl. Electrochem.*, 30, 1345 (2000). Copyright 2000, Kluwer Academic.

the presence of carboxylic acids is a decrease in the starting potential of water discharge and/or decomposition of the supporting electrolyte. Figures 24 and 25 show typical voltammograms obtained with formic and oxalic acid by the workers (Gandini, Mahé, Michaud, Haenni, Perret and Comninellis, 2000).

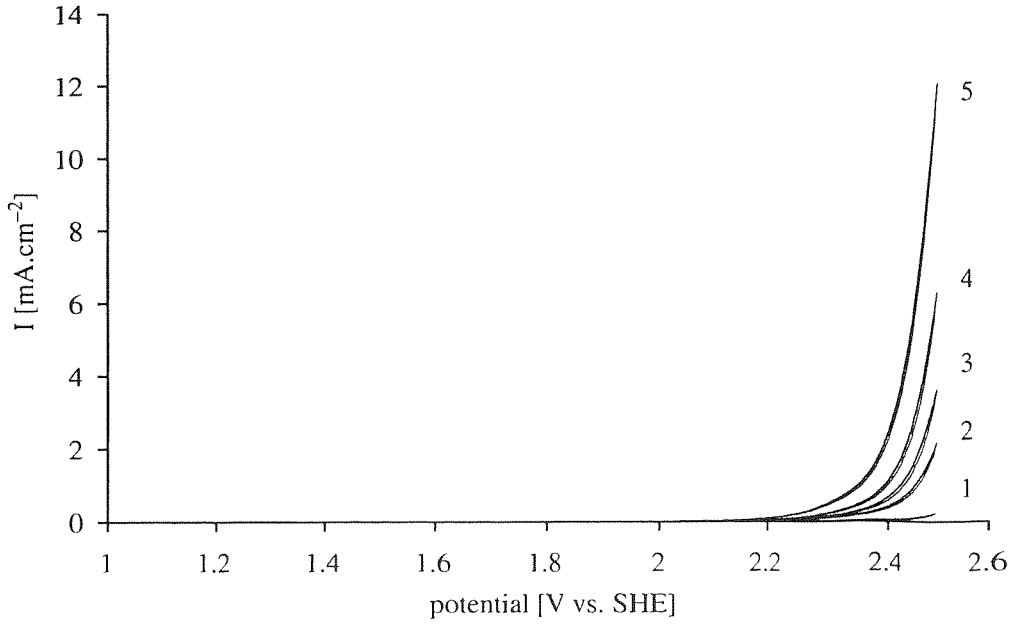

FIG. 25. Cyclovoltammograms of BDD (1) in 1 M H_2SO_4, (2) in 1 M H_2SO_4 + 0.05 M oxalic acid, (3) in 1 M H_2SO_4 + 0.1 M oxalic acid, (4) in 1 M H_2SO_4 + 0.2 M oxalic acid and (5) in 1 M H_2SO_4 + 0.5 M oxalic acid. Scan rate: 50 mV s^{-1}, $T = 25$ °C. Reprinted with permission from: D. Gandini, E. Mahé, P.-A. Michaud, W. Haenni, A. Perret, and Ch. Comninellis, *J. Appl. Electrochem.* 30, 1345 (2000). Copyright 2000. Kluwer academic.

For both carboxylic acids the current density at a given potential in the region of decomposition of the supporting electrolyte amplifies with increasing carboxylic acid concentration. This may indicate that the pathway for the oxidation of these carboxylic acids involves intermediates that are formed during decomposition of water and/or the supporting electrolyte (indirect mechanism).

The following reaction schema can be proposed for the oxidation of carboxylic acids on BDD anodes:

- formation of hydroxyl radicals (OH) on BDD surface by water discharge (Eq. (11))

$$BDD(H_2O) \rightarrow BDD(OH) + H^+ + e^- \quad (11)$$

- oxidation of carboxylic acid by the electro-generated hydroxyl radicals at the BDD (Eq. (12)).

$$BDD(OH) + \text{carboxylic acids} \rightarrow BDD + CO_2 + H_2 \quad (12)$$

The main side effects during the anodic oxidation of organics in H_2SO_4 are oxygen evolution, H_2O_2 and $H_2S_2O_8$ formation.

6.2.2. *Oxidation of Phenolic Compounds in the Potential Region of Water Stability*

Voltammetric measurements of phenolic compounds (phenol, chlorophenol and β-naphtol) have shown that in the potential region before oxygen evolution, an anodic peak is obtained due to oxidation of the phenolic compound to the corresponding phenoxy radical according to the findings of these workers (Gandini et al., 2000).

This anodic reaction can induce polymerization resulting in the deposition of adhesive polymeric material on the electrode surface. The formation of these polymeric material results in electrode deactivation following these workers (Iniesta et al., 2001b).

Washing with organic solvents (isopropanol) does not reactivate the electrode. However, the electrode surface can be restored to its initial activity by an anodic polarization in the same electrolyte in the potential region of water decomposition ($E > 2.3$ V vs. SHE). In fact, this potential is in the region of water discharge. On BDD it involves the production of active intermediates, probably hydroxyl radicals that oxidize the polymeric film present on the electrode surface.

The electrode deactivation by polymeric materials and reactivation at high anodic potentials can be illustrated using phenol as a model phenolic compound.

Figure 26 shows typical cyclic voltammetric curves for BDD electrodes obtained in a solution containing 2.5 mM of phenol in 1 M $HClO_4$ at a scan rate of 100 mV s^{-1}.

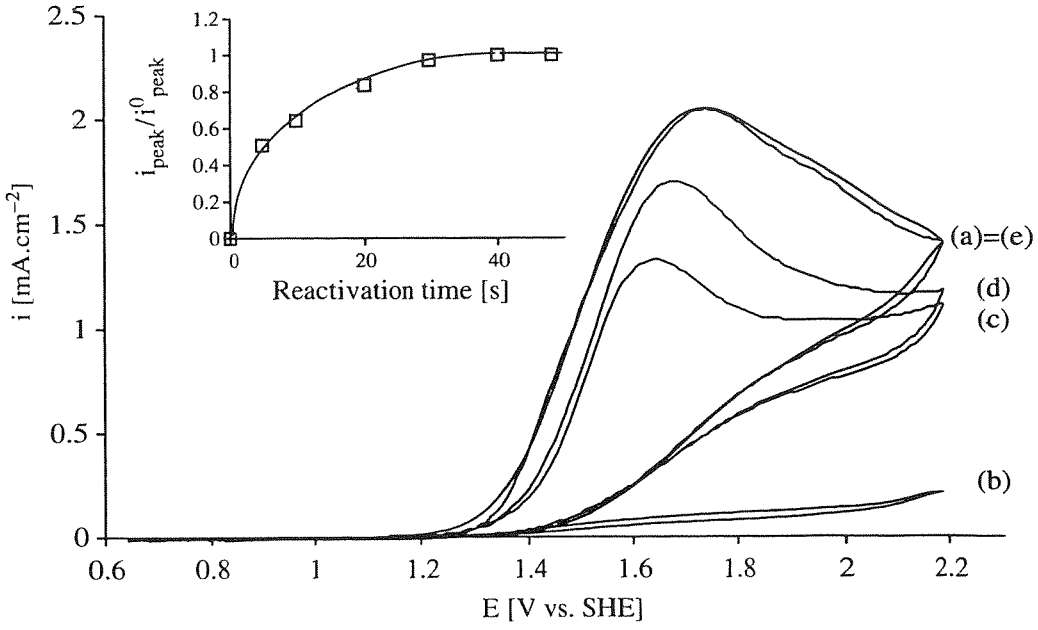

FIG. 26. Cyclic voltammograms on BDD for 2.5 mM phenol solution in 1 M $HClO_4$. (a) First cycle; (b) after 5 cycles; (c) after reactivation at +2.84 V vs. SHE for 10 s; (d) after reactivation at +2.84 V vs. SHE for 20 s; (e) after reactivation at +2.84 V vs. SHE for 40 s. Scan rate: 100 mV s^{-1}, $T = 25$ °C. Inset: dependence of the normalized current peak (i_{peak}/i^0_{peak}, where i^0_{peak} is the current peak during the first scan) during the reactivation. Reprinted with permission from: M. A. Rodrigo, P.-A. Michaud, I. Duo, M. Panizza, G. Gerisola, and Ch. Comninellis, *J. Electrochem. Soc.* 148 (5), D60 (2001). Copyright 2001. The Electrochemical Society Inc.

In the first scan (curve a, Fig. 26) an anodic current peak corresponding to the oxidation of phenol is observed at about 1.65 V. As the number of cycles increases, the anodic current peak decreases to almost zero after about five cycles (curve b, Fig. 26). The same figure shows the voltammetric responses obtained after electrode reactivation at the fixed anode potential of 2.84 V vs. SHE for 10, 20 and 40 s (curve c, d, e, Fig. 26).

The trend of the normalized current peaks (i_{peak}/i^0_{peak}, where i^0_{peak} is the current peak during the first scan) as a function of polarization time at 2.84 V vs. SHE is given in the inset in Figure 26.

Figure 26 shows clearly that when the polarization time during electrode reactivation exceeds 40 s, the phenol oxidation peak comes back to its initial position, meaning that the electrode is restored to its initial activity according to the findings of these workers (Gherardini, Michaud, Panizza, Comninellis and Vatistas, 2001).

6.2.3. *Oxidation of Organic Compounds on BDD at High Anodic Potential*

The electrochemical oxidation of a large number of organic compounds (Table VII) at high anodic potential (close to the potential region of supporting

TABLE VII

INVESTIGATED ORGANIC COMPOUNDS ON BDD ANODE

Carboxylic acids
Acetic, formic, maleic and oxalic
Alcohols and ketones
Methanol, ethanol, isopropanol, acetone
Phenolic compounds
Phenol, *p*-chlorophenol, β-naphthol
Aromatic acids
Benzoic acid, benzene sulfonic acid, nicotinic acid
Soluble polymers
Polyacrylic acid

electrolyte/water decomposition) on BDD has shown that the oxidation can be achieved at high current efficiency without any indication of electrode deactivation (this was the case for phenolic compounds at low anodic potentials) (Gherardini et al., 2001; Iniesta et al., 2001b).

Furthermore, the oxidation products depend on the experimental conditions. In fact, it has been found that the partial oxidation of the organic compound for electroorganic synthesis or the complete oxidation for wastewater treatment can be obtained.

In particular, when working at high current density (above the limiting current for the complete combustion given by Eq. (13)), complete oxidation of the organic compound can be achieved.

$$i_{\text{lim}}(t) = 4Fk_{\text{m}}\text{COD}(t) \tag{13}$$

where

$i_{\text{lim}}(t)$	limiting current (A m^{-2}) at a given time t,
4	number of exchanged electrons,
F	Faraday's constant (C mol^{-1}),
k_{m}	average mass transport coefficient (m s^{-1}),
COD(t)	chemical oxygen demand (mol O_2 m^{-3}) at time t.

A theoretical model has been developed permitting prediction of the chemical oxygen demand (COD) and instantaneous current efficiency (ICE) during the electrochemical oxidation of organic pollutants on BDD electrodes in a batch recirculation system under galvanostatic conditions.

The model assumes that the rate of the electrochemical oxidation of the organic compounds (main reaction) is a fast reaction in relation to the oxygen evolution reaction (side reaction).

Depending on the applied current density and the limiting current density (Eq. (13)), two different operating regimes have been identified:

$i_{appl.} < i_{lim}$ the electrolysis is under current control, the current efficiency is 100% and the COD decreases linearly with time.

$i_{appl.} > i_{lim}$ the electrolysis is under mass transport control, side reactions (such as oxygen evolution) are involved, resulting in a decrease of ICE. In this regime the COD removal, due to mass-transport limitation, follows an exponential trend.

The equations that describe the temporal trends of COD and ICE in both regimes are summarized in Table VIII.

The model has been tested for different classes of organic compounds (Table VII). For almost all the organic compounds investigated there is a good agreement between the model and the experimental data.

The ICE has been obtained through the measurement of the COD using relation (14):

$$\mathrm{ICE} = 4FV\frac{[(\mathrm{COD})_t - (\mathrm{COD})_{t+\Delta t}]}{I\Delta t} \tag{14}$$

where

$(\mathrm{COD})_t$ chemical oxygen demand at time t (mol O_2 dm^{-3})
$(\mathrm{COD})_{t+\Delta t}$ COD at time $t + \Delta t$ (mol O_2 dm^{-3})
I current (A)
F Faraday constant (26.8 A h)
V volume of electrolyte (dm^3)
Δt interval time of COD measurement (h)

TABLE VIII

EQUATIONS DESCRIBING COD AND ICE EVOLUTION DURING OXIDATION AT BDD ELECTRODE

	Instantaneous current efficiency (−)	Chemical oxygen demand (mol O_2 m^{-3})
$i_{appl.} < i_{lim}$ under current limited control	$\mathrm{ICE} = 1$	$\mathrm{COD}(t) = \mathrm{COD}^0\left(1 - \frac{\alpha A k_m}{V_R}t\right)$
$i_{appl.} > i_{lim}$ under mass transport control	$\mathrm{ICE} = \exp\left(-\frac{Ak_m}{V_R}t + \frac{1-\alpha}{\alpha}\right)$	$\mathrm{COD}(t) = \alpha\mathrm{COD}^0\exp\left(-\frac{Ak_m}{V_R}t + \frac{1-\alpha}{\alpha}\right)$

V_R = Reservoir volume (m^3), k_m = Mass-transfer coefficient ($m\ s^{-1}$), A = Electrode area (m^2), COD^0 = Initial chemical oxygen demand (mol O_2 m^{-3}), $\alpha = i/i^0_{lim}$.

Reprinted with permission from: M. A. Rodrigo, P.-A. Michaud, I. Duo, M. Panizza, G. Gerisola, and Ch. Comninellis, *J. Electrochem. Soc.*, 148 (5), D60 (2001). Copyright 2001. The Electrochemical Society Inc.

A typical example is shown in Figure 27. Both theoretical and experimental COD and ICE trends are given for the anodic oxidation of 4-chlorophenol at BDD anode. As can be seen, the model is in good agreement with the experimental data. Similar results are obtained for almost all the organic compounds investigated (Table VII).

6.2.4. *Practical Applications*

Wastewaters from automotive, chemical, paper and pigment industry were successfully treated with very low operating cost in the case of no mass transport limitations according to the findings of these workers (Fryda, Dietz, Herrmann, Hampel, Schäfer, Klages, Perret, Haenni, Comninellis and Gandini, 2000; Kraft et al., 2001). One example of a practically relevant wastewater stems from the automotive industry. It is a condensate from a cooling-lubricant cycle in motor production. In Figure 28 the COD reduction and current efficiency for an electrochemical advanced oxidation process (EAOP) are shown. The investigation is carried out in a monopolar mesh reactor cell (Fig. 13) with a stack of 1 m^2 of diamond grid electrodes at a distance of 4 mm. The decrease of COD with increasing charge is linear to 500 mg O_2 l^{-1}. The current efficiency is better than 90% for

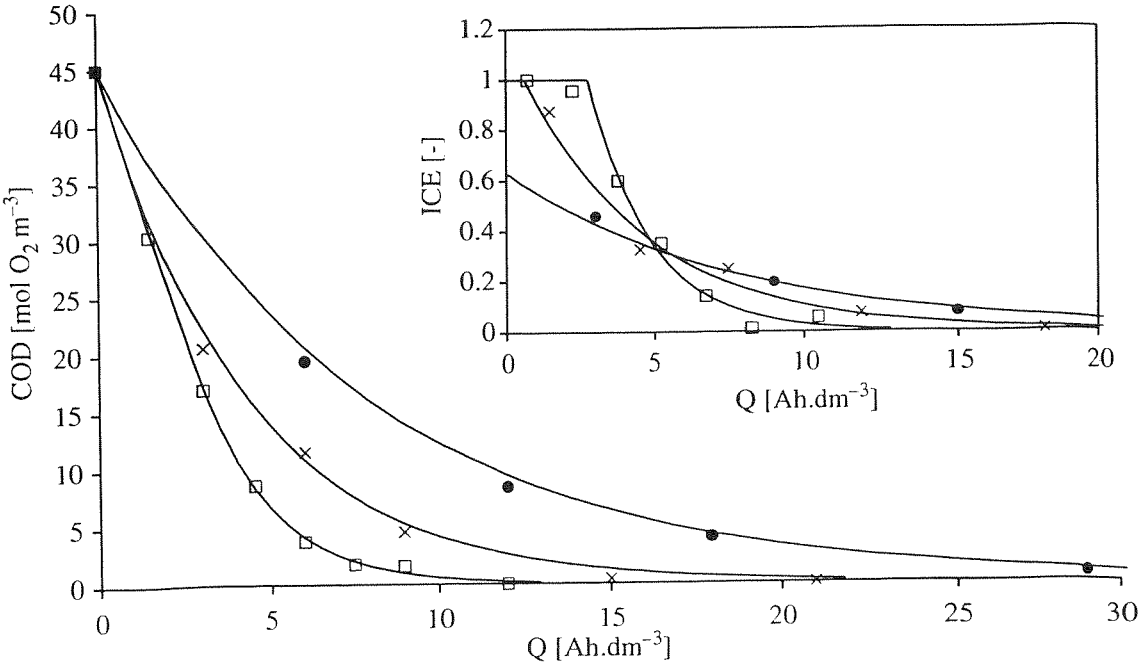

FIG. 27. Influence of 4-CP concentration on the evolution of COD and ICE (inset) with the specific electrical charge passed during the electrolyses on a BDD anode. Electrolyte: sulfuric acid 1 M; $T = 25$ °C; applied current density = 30 mA cm^{-2}; initial 4-CP concentration: (□) 3.9 mM; (×) 7.8 mM; (●) 15.6 mM. The solid lines represent model prediction. Reprinted with permission from: M. A. Rodrigo, P.-A. Michaud, I. Duo, M. Panizza, G. Gerisola, and Ch. Comninellis, *J. Electrochem. Soc.*, 148 (5), D60 (2001). Copyright 2001. The Electrochemical Society Inc.

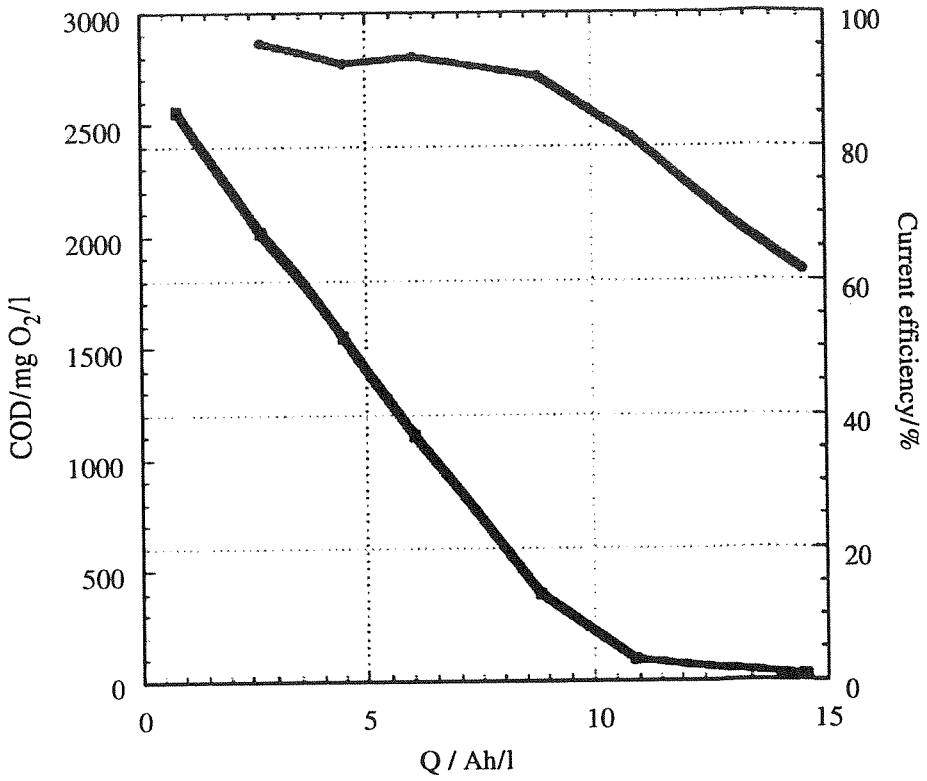

FIG. 28. Efficient decomposition of organics in an oil containing waste water (condensate) from automotive industry applying EAOP. EAOP treatment was performed by GERUS GmbH, Berlin.

COD values and higher than 500 mg $O_2\,l^{-1}$. For lower COD values the high current efficiency decreases slowly to 50% for values about 25 mg $O_2\,l^{-1}$ due to mass transport limitations in the electrochemical cell. In this pilot treatment EAOP yields nearly the same results as achieved in laboratory scale investigations. During several weeks of oxidation the properties of the diamond electrodes have not been affected and poisoning of the surface is not detectable. However, the extremely high oxidation potential of EAOP yields unspecific side reactions, for example formation of nitrate, chlorate or AOX, which must be considered in the construction of electrochemical water treatment devices with diamond electrodes.

6.2.5. *Economic Considerations*

The specific energy consumption (E_{sp}), expressed in kW h kg COD^{-1}, for the electrochemical treatment can be estimated from relation (15) following Comninellis (1992):

$$E_{sp} = 3.35\frac{V_c}{\overline{\eta}} \tag{15}$$

where V_c is the cell potential (in Volt) and $\overline{\eta}$ the average current efficiency.

The average current efficiency ($\bar{\eta}$) can be calculated from the ICE–time (or ICE–A h l^{-1}) curve using relation (16) according to the findings of these workers (Panizza, Michaud, Cerisola and Comninellis, 2001):

$$\bar{\eta} = \frac{\int_0^{\tau} \mathrm{ICE} \cdot \mathrm{d}t}{\tau} \tag{16}$$

where τ is the duration of the electrochemical treatment in order to achieve a given degree of COD elimination.

The required electrode surface area A (m^2) for the electrochemical elimination of a given loading P (kg COD h^{-1}) can be calculated from relation (17):

$$A = 3.35 \frac{P}{i \cdot \bar{\eta}} \tag{17}$$

where i is the applied current density (kA m^{-2}).

6.3. Electrochemical Treatment of Waste Water Containing Cyanides

Whenever cyanides are manufactured or used, effluents and wastes containing various amounts of cyanide are produced. Because of the high toxicity of cyanide to all forms of life the effluents and wastes must be treated to reduce its content to acceptable concentrations. Depending on the quantity and type of cyanide waste, various detoxification methods are used. In addition to effectiveness and cost, the formation of undesirable byproducts and additional salting of the wastewater are factors of growing importance in choosing a treatment method.

Alkaline chlorination is the most frequently used process for the treatment of effluents containing < 1 g CN^- l^{-1}. The treatment can be carried out with chlorine and alkali [NaOH, $Ca(OH)_2$] or with hypochlorite solutions that contain about 12% NaOCl.

The main disadvantages of this method are:

- poisonous ClCN gas evolution during treatment
- use of dangerous chemicals (Cl_2, NaOCl) and additional salting of the water
- high operation cost.

The electrochemical oxidation of cyanide may overcome these disadvantages. The cyanide can directly be oxidized on the anode (direct electrochemical oxidation) or indirectly by electro-generated hypochlorite (indirect electrochemical oxidation).

The detailed mechanism of the direct electrochemical oxidation of cyanide is still controversial, but it has generally been accepted that the first step is

the electrochemical oxidation of cyanide to cyanate, which is further oxidized in a much slower and complex reaction to form urea, oxalate, carbonate and nitrogen.

In the indirect electrochemical process, chloride ion (present in the wastewater or introduced in catalytic amount) acts as an oxygen carrier (forming ClO) in the oxidation of cyanide to cyanate (Eq. (18)).

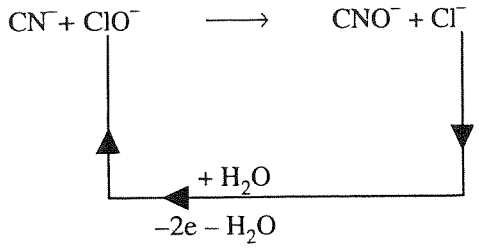

(18)

The main problem with the electrochemical treatment of cyanide is the low stability of the anodes used (graphite, Pb, IrO_2, RuO_2, etc.) and the low current efficiency.

Preliminary measurements using BDD anodes for the direct electrochemical oxidation of cyanide have shown that very high current efficiencies (>90%) can be achieved for concentrated cyanide solutions (>0.5 M) according to the findings of these workers (Kraft et al., 2000). However, the current efficiency decreases strongly with diminishing the cyanide concentration. This is mainly due to mass transfer limitations.

With the indirect electrochemical process using chloride as mediator the efficiency of the process can be greatly increased as demonstrated by the authors (Fryda et al., 1999b).

In Table IX the influence of chloride concentration on the specific energy consumption (kW h m^{-3}) for the treatment of a solution containing 8 mg CN^- l^{-1} in 0.1 M KOH (90% elimination of CN^-) using BDD anodes at 25 °C is given. This table clearly shows the dramatic decrease in the specific energy consumption with increasing chloride concentration.

6.4. Disinfection of Swimming Pool Water

As was demonstrated in Section 5.3 BDD-electrodes can produce hydroxyl radicals, which may also be responsible for the production of chlorine, persulfates, ozone and hydrogen peroxide at high yields. It was also

TABLE IX

Influence of Cl^- Concentration on the Specific Energy Consumption for the Treatment of a Solution Containing 8 mg CN^- L^{-1} (90% Elimination of CN^-) Using BDD Anodes

Conc. Cl^- (mM)	0	10	50	100
kW h m^{-3}	16.5	4.5	1.1	0.5

established in a previous section that all tested organics, and until today there are no visible limits, can be oxidized electrochemically to CO_2 and water. Therefore, it has been useful to test the performance of BDD-electrodes for disinfection of swimming pool water according to findings of these workers (Lorenz et al., 2000).

As all natural waters contain small amounts of various mineralizations like chlorides, sulfates, hydrogen carbonates, the electrochemical formation of oxidants, which are also disinfectants, is possible.

It has been shown in a swimming pool experiment (60 m^3) that oxidizing compounds can disinfect water. In fact, fresh water containing 250 ppm of sodium chloride and 0.2 ppm of free chlorine, produced either electrochemically or by adding NaOCl, destroyed 1×10^6 *E. coli* cm^{-3} in a period of 20 or 60 min, respectively (Fig. 29). As bacteria and virus are killed with a much higher efficiency by the electrochemical disinfection method than with the standard hypochloride method, it is supposed that not only chlorine but other disinfectants like ozone and hydrogen peroxide are formed and remain in the water. They are even more powerful disinfectants.

The chlorine concentration in the water was measured by means of a new type of a direct (no diaphragm) and highly selective sensor, which is loop-controlled by a microprocessor in the range of 0.05–1 ppm. A similar system is under test for ozone production.

In conclusion, we have shown that the use of diamond electrodes with loop control, for the electrochemical production of oxidizing agents such as chlorine

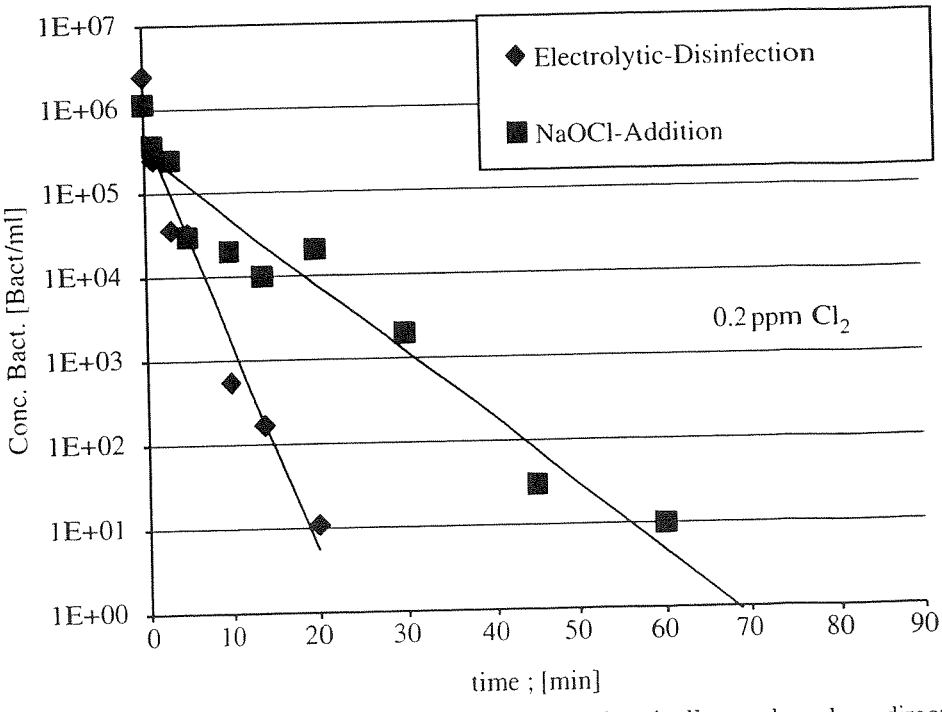

FIG. 29. Comparison of the effect on *E. coli* of electrochemically produced or directly added hypochlorite (NaOCl) solution at a concentration of 0.2 ppm active chlorine.

and ozone, is a highly efficient method for the disinfection of water according to the findings of these workers (Kraft et al., 2000; Lorenz et al., 2000).

Acknowledgements

The authors would like to thank Ilaria Duo, Boris Correa and Pierre-Alain Michaud at EPFL, Markus Gurk at University of Neuchâtel, Jürg Wurm at METAKEM, Thomas Lehmann at INFRACOR, Alexander Kraft at GERUS GmbH, Lothar Schäfer at FhG-IST, André Perret at CSEM for their collaboration as well as Karin Chabloz and Claudine Julia-Schmutz at CSEM for reviewing.

References

E. Abdelmula and K. Jüttner, "Characterization of DiaChem® Electrodes by Electrochemical Impedance Spectroscopy." 4th Workshop on Diamond Electrodes, Braunschweig, Germany, 2001.

P. Andrezza, M. I. De Barros, C. Andrezza-Vignolle, D. Rats, and L. Vandenbulcke, In-depth structural X-ray investigation of PECVD grown diamond films on titanium alloys, *Thin Solid Films* 319, 62–66 (1998).

F. Beck, W. Kaiser, and H. Krohn, Boron doped diamond (BDD)-layers on titanium substrates as electrodes in applied electrochemistry, *Electrochim. Acta* 45, 4691–4695 (2000).

C. Comninellis, Traitement des eaux résiduaires par voie électrochimique, *GWA* 11/92, 792–797 (1992).

C. Comninellis, P.-A. Michaud, W. Haenni, A. Perret, and M. Fryda, Elektrochemische Herstellung von Peroxodischwefelsäure unter Einsatz von diamantbeschichteten Elektroden. Patent DE 199 48 184 A1, 1999.

A. Densienko, A. Aleksov, and E. Kohn, PH-sensing by surface-doping diamond and effect of the diamond surface termination, *Diamond Relat. Mater.* 10, 667–672 (2001).

I. Duo, P.-A. Michaud, W. Haenni, A. Perret, and Ch. Comninellis, Activation of boron doped diamond with IrO_2 clusters, *Electrochem. Solid-State Lett.* 3, 325 (2000).

S. Ferro, A. De Battisti, I. Duo, Ch. Comninellis, W. Haenni, and A. Perret, Chlorine evolution at highly boron doped diamond electrodes, *J. Electrochem. Soc.* 147, 2614–2619 (2000).

V. Fischer, D. Gandini, S. Laufer, E. Blank, and Ch. Comninellis, Preparation and characterization of Ti/diamond electrodes, *Electrochim. Acta* 44, 521 (1998).

M. Fryda, A. Dietz, D. Herrmann, A. Hampel, L. Schäfer, C.-P. Klages, A. Perret, W. Haenni, C. Comninellis, and D. Gandini, Wastwatertreatment with diamond electrodes, *Electrochem. Proc. Vol.* 99–32, 473–483 (2000).

M. Fryda, A. Hampel, D. Hermann, L. Schäfer, and C.-P. Klages, Eigenschaften und Anwendungen von Diamantelektroden, *J. für Oberflächentechnik* 5/99, VI–IX (1999a).

M. Fryda, D. Hermann, L. Schäfer, C.-P. Klages, A. Perret, W. Haenni, Ch. Comninellis, and D. Gandini, Properties of diamond electrodes for waste water treatment, *New Diamond Frontier Carbon Technol.* 9, 229–240 (1999b).

Y. Fu, B. Yan, and N. L. Loh, Effect of pre-treatments and interlayers on the nucleation and growth of diamond coatings on titanium substrates, *Surf. Coat. Technol.* 130, 173–185 (2000).

Y. Fu, B. Yan, N. L. Loh, C. Q. Sun, and P. Hing, Deposition of diamond coatings on pure titanium using micro-wave plasma assisted chemical vapor deposition, *J. Mater. Sci.* 34, 2269–2283 (1999).

D. Gandini, E. Mahé, P.-A. Michaud, W. Haenni, A. Perret, and Ch. Comninellis, Oxidation of carboxylic acids on boron doped diamond electrodes, *J. Appl. Electrochem.* 30, 1345–1350 (2000).

L. Gherardini, P.-A. Michaud, M. Panizza, Ch. Comninellis, and N. Vatistas, Electrochemical oxidation of 4-chlorophenol for waste water treatment. Definition of normalized current efficiency, *J. Electrochem. Soc.* 148, D78–D82 (2001).

M. Gurk, "Experimental Data". University of Neuchâtel, Geomagnetism Group, Neuchâtel, Switzerland, 2001.

W. Haenni, M. Borel, A. Perret, B. Correa, P.-A. Michaud, and Ch. Comninellis, "Production of Oxidants on Diamond Electrodes." In Scientific report CSEM Switzerland, 70, 1999a.

W. Haenni, C. Faure, and P. Rychen, Modular electrochemical cell. Patent WO 02/088430 A1, 2001a.

W. Haenni and M. Fryda, "Substrates for Diamond Electrodes." 3rd Workshop on Diamond Electrodes, Neuchâtel, Switzerland, 2000a.

W. Haenni and A. Perret, Procédé de depot d'une couche de diamant sur un metal réfractaire de transiston et pièce revêtue d'une telle couche. Patent F 2 790 267, 1999b.

W. Haenni and A. Perret, Electrolytic cell with bipolar electrode including diamond. Patent US 6 306 270 B1, 2000b.

W. Haenni, A. Perret, and P. Rychen, Electrodes de grandes dimensions. Patent EP 1 229 149 A1, 2001b.

G. Heinrich, T. Grögler, S. M. Rosiwal, R. F. Singer, R. Stöckel, and L. Ley, The influence of diamond chemical vapor deposition coating parameters on the microstructure and properties of titanium substrates, *Diamond Relat. Mater.* 5, 304–307 (1996).

J. Iniesta, P.-A. Michaud, M. Panizza, G. Cerisola, A. Aldaz, and Ch. Comninellis, Electrochemical oxidation of phenol on boron doped diamond electrodes, *Electrochim. Acta* 46, 3573 (2001a).

J. Iniesta, P.-A. Michaud, M. Panizza, and Ch. Comninellis, Electrochemical oxidation of 3-methylpyridin on boron doped diamond electrodes. Application to electro-organic synthesis and waste water treatment, *Electrochem. Commun.* 3, 346–351 (2001b).

W. Jiali, Z. Jianzhong, Z. Guoxiong, L. Xinru, and C. Nianyi, Fabrication and application of a diamond-film glucose biosensor based on a H_2O_2 microarray electrode, *Anal. Chim. Acta* 327, 133–137 (1996).

N. Katsuki, E. Takahashi, M. Toyoda, T. Kurosu, M. Lida, S. Wakita, Y. Nishiki, and T. Shimamune, Water electrolysis using diamond thin film electrodes, *J. Electrochem. Soc.* 145, 2358–2362 (1998).

A. Kraft, M. Stadelmann, and W. Kirstein, Einsatz von Diamantelektroden für die elektrolytische Wasserreinigung und -desinfektion durch anodische Oxydation, *Galvanotechnik* 91, 334–339 (2000).

A. Kraft, M. Stadelmann, and M. Blaschke, "Examples for Electrochemical Water Treatment Using Diamond Electrodes." 4th International Workshop Diamond Electrodes, Braunschweig, Germany, 2001.

T. Lehmann, "Application of BDD-electrodes in Electrochemical Processes." 3rd Workshop on Diamond Electrodes, Switzerland, 2000a.

T. Lehmann, "Elektrochemische Umsetzung mit dotierten Diamantschichtelektroden." GdCh-Tagung Angewandte Elektrochemie, Ulm, Germany, 2000b.

J. Lorenz, L. Pupunat, Ch. Comninellis, B. Correa, W. Haenni, and A. Perret, "Disinfection of Water Using Boron Doped Diamond Electrodes." 51st Annual ISE Meeting, Warsaw, Poland, Abstract 228, 2000.

C. Madore, A. Duret, W. Haenni, and A. Perret, "Detection of Trace Silver and Copper at an Array of Boron-doped Diamond Microdisk Electrodes." Proceedings of the Symposium on Microfabricated Systems and MEMS, The Electrochemical Society Proceedings Series Pennington, NJ. (P.J. Mesketh, H. Hughes, and W. E. Bailey, Eds.) PV, 2000-19, p. 159, 2000.

H. B. Martin, A. Argoitia, J. C. Angus, A. B. Anderson, and U. Landau, "Boron Doped Diamond Electrodes for Electrochemical Applications." In Applications of Diamond Films and Related Materials: Third International Conference. (A. Feldman, Y. Tzeng, W. A. Yarbrough, M. Yoshikawa, M. Murakawa, Eds.) NIST Special Publication, Vol. 885, pp. 91–94, 1995.

P.-A. Michaud, E. Mahé, W. Haenni, A. Perret, and Ch. Comninellis, Preparation of peroxodisulfuric acid using boron doped diamond thin film electrodes, *Electrochem. Solid-State Lett.* 3, 77–79 (2000).

M. Panizza, I. Duo, P.-A. Michaud, G. Cerisola, and Ch. Comninellis, Electrochemical detection of 2-naphtol on boron doped diamond. Influence of anodic treatment, *Electrochem. Solid-State Lett.* 3, 429 (2000a).

M. Panizza, I. Duo, P.-A. Michaud, G. Cerisola, and Ch. Comninellis, Electrochemical generation of silver (II) on boron doped diamond electrodes, *Electrochem. Solid-State Lett.* 3, 550–551 (2000b).

M. Panizza, P.-A. Michaud, G. Cerisola, and Ch. Comninellis, Electrochemical treatment of waste water containing organic pollutants on boron doped diamond electrodes. Prediction of specific energy consumption and required electrode, *Electrochem. Commun.* 3, 336–339 (2001).

A. Perret, W. Haenni, P. Niedermann, N. Skinner, Ch. Comninellis, and D. Gandini, Diamond electrodes and microelectrodes, *Electrochem. Soc. Proc.* 97, 275–283 (1997).

F. E. Perrier, G. Petiau, G. Clerc, V. Bogorodsky, E. Erkul, L. Jouniaux, D. Lesmes, J. Macnae, J. M. Meunier, D. Morgan, D. Nascimento, G. Oettinger, G. Schwarz, H. Toh, M. J. Valiant, K. Vozoff, and O. Yazici-Cakin, A one year systematic study of electrodes for long period measurements of electric field in geophysical environments, *J. Geomag. Geoelectr.* 49, 1677 (1997).

H. Pütter, A. Weiper-Idelmann, and C. Merk, Diamantbeschichtete Elektroden. Patent DE 1991 17 46, and EP 1 036 861 A1, 1999.

R. Ramesham, Differential pulse voltammetry of toxic metal ions at the boron-doped CVD diamond electrode, *J. Mater. Sci.* 34, 1439–1445 (1999a).

R. Ramesham, Voltammetric studies at the polycrystalline diamond grown over a graphite electrode material, *Thin Solid Films* 339, 82–87 (1999b).

P. Rychen, J. Gobet, and C. Madore, "Electrochemical Sensors for Environmental Systems." 4th Workshop Diamond Electrodes, May 2001, Braunschweig, Germany.

A. Y. Sakharova, Y. V. Pleskov, F. Di Quarto, S. Piazza, C. Sunseri, I. G. Teremetskaya, and V. P. Varnin, Synthetic diamond electrodes: photoelectrochemical investigation of undoped and boron-doped polycrystalline thin films, *Electrochem. Soc.* 142, 2704 (1995).

G. M. Swain, The susceptibility to surface corrosion in acidic fluoride media—a comparison of diamond, HOPG, and glassy carbon electrodes, *J. Electrochem. Soc.* 141, 3382–3393 (1994).

G. M. Swain, A. B. Anderson, and J. C. Angus, Application of diamond thin films in electrochemistry, *MRS Bull. Sept.*, 57–59 (1998).

N. Vinokur, B. Miller, N. Vinokur, B. Miller, Y. Avyigal, and R. Kalish, Electrochemical behavior of boron doped diamond electrodes, *J. Electrochem. Soc.* 143, L238 (1996).

J. Wurm, "The use of Diamond Coated Anodes for Chromium Plating." 3rd International Colloquium on Hard and Decorative Chromium Plating, St. Etienne, France, pp. 25–27, 2001.

J. Wurm, M. Fryda, and L. Schäfer, Gebrauchsmusterschrift DE 299 16 125 U1, 1999.

T. Yano, D. A. Tryk, K. Hashimoto, and A. Fujishima, Electrochemical behavior of highly conductive boron-doped diamond films grown by chemical vapor deposition, *J. Electrochem. Soc.* 145, 1870–1876 (1998).

B. D. Yu, Y. Miyamoto, and O. Sugino, Efficient n-type doping of diamond using surface-mediated epitaxial growth, *Appl. Phys. Lett.* 76, 976–978 (2000).